Transportation Research Part D 89 (2020) 102584

Contents lists available at ScienceDirect

Transportation Research Part D

journal homepage: www.elsevier.com/locate/trd

A spatiotemporal analysis of the robustness of high-speed rail network in China

Jingjuan Jiao [a], Fangni Zhang [b,*], Jian Liu [c,*]

[a] School of Economics and Management, Beijing Jiaotong University, Beijing 100044, China
[b] Department of Industrial and Manufacturing Systems Engineering, University of Hong Kong, Hong Kong, China
[c] School of Computer and Information Technology, Beijing Jiaotong University, Beijing 100044, China

ARTICLE INFO

Keywords:
High-speed rail
Network capacity
Weighted network efficiency
Robustness
Spatiotemporal variation

ABSTRACT

Most studies on the robustness of high-speed rail (HSR) network examine the issue at the aggregate level and consider a fixed period (e.g., a day or a month), regardless of when and where the disruption occurs. This study proposes a holistic framework of assessing the impact of node cascading disruptions in HSR network considering different affected times-of-day and geographic regions. A weighted network efficiency metric is proposed to assess network performance considering both travel time and train frequency along the topological shortest path. Analysis of China's HSR finds that (1) the network is less robust to disruptions occurring in East China or along the Harbin-Hong Kong corridor; (2) Disruptions during 10:00–15:00 have the largest impact; (3) lockdowns during COVID-19 outbreak in Jan-Feb 2020 led to 14.5% reduction in overall network efficiency. The results generate insights into further development of the HSR network and provide policy support for HSR resilience-enhancing strategies.

1. Introduction

High-speed railway (HSR) is a crucial transport infrastructure and plays a growing role in intercity travels in many countries around the world. The HSR network may face different types of disturbances such as natural hazards (e.g. typhoon and continuous snowfall), technological failures (e.g. device fault), and man-made failures (e.g. cyber-attack), which may result in significant travel delays, reduced accessibility, unexpected detour and transfers, and even loss of lives, causing enormous economic loss and/or serious fatality (Wang et al., 2015). For example, influenced by the Coronavirus Disease 2019 (COVID-19), all HSR stations in Wuhan City, the capital of Hubei Province, were forced to shut down from 23 January 2020 to 8 April 2020, which largely affected the performance of the HSR network in China. It is our urgent need to understand the robustness of the HSR network and minimize the negative impacts of HSR disruptions on passengers and economic losses.

Robustness, the opposite of vulnerability, has long been a central issue in transportation and is traditionally defined as the ability to retain its performance under disruptions and attacks (Sullivan et al., 2010; Lordan and Albareda-Sambola, 2019; Li and Rong, 2020; Chen et al., 2020). Robustness is widely used to explore the network performance of transportation systems under disruptions, especially the air transport (Pien et al., 2015), urban road network (Zhang et al., 2013; Tang and Huang, 2019; Sun et al., 2018), urban rail system (Sun et al., 2018; Yang et al., 2019; Yap et al., 2018), port (Cao and Lee, 2019), and railway system (Hong et al., 2019; Ye and Kim, 2019).

* Corresponding authors.
E-mail addresses: fnzhang@hku.hk (F. Zhang), jianliu@bjtu.edu.cn (J. Liu).

https://doi.org/10.1016/j.trd.2020.102584

Available online 4 November 2020

The metrics of network performance in the previous literature can be divided into three types, namely the topology-based, service-based, and the location-based metrics (Tang and Huang, 2019; Li and Rong, 2020). The first type of metric only measures the connectivity in the topological network that describes the physical network. The metrics often involve the size of the giant component, the average size of the isolated clusters and network efficiency (Chen et al., 2020), and the degree and betweenness centrality (Erath et al., 2009). The second type focuses on the evaluation of transportation function considering traffic characteristics, including the number of canceled trains (Vansteenwegen et al., 2016), the delay of passengers (Adjetey-Bahun et al., 2016; Khaled et al., 2015), and changes in passenger flow (Jiang et al., 2018). The third type of metrics incorporates connectivity or accessibility indicators in the geographical network, e.g., the average travel time (Rodríguez-Núñez and García-Palomares, 2014). Some scholars pointed out that the importance of a station or a link depends not only on topology attributes but also on the service level and their location in the network. For example, Erath et al. (2009) estimated the robustness of the railway in Switzerland using both the topology-based indicators i.e. degree and closeness centrality, and the location-based indicator i.e. travel time. Some studies also incorporated the service-based indicators, i.e., number of trains, delay of passengers, and the location-based indicators, i.e. travel time, to evaluate the robustness of various transport networks (Rodríguez-Núñez and García-Palomares, 2014; Cats et al., 2017; Yin et al., 2016). These methods are also widely used in the analysis of other network systems, e.g., the water distribution system (Yazdani et al., 2011; Meng et al., 2018) and power grid (Zhang et al., 2014).

With the recent development of HSR, there is a growing interest in the robustness of HSR networks (Zhang et al., 2016; Janić, 2018; Li et al., 2019; Chen and Wang, 2019; Li and Rong, 2020). Previous researches mainly concentrate on the robustness of the HSR network in a fixed period (a day or a month). However, disruptions and failures may occur at any time, last for long or short, and can happen anywhere[1]. Although some researchers began to explore the robustness from the time and space-dynamic perspectives (Hong et al., 2019; Li and Rong, 2020), the following questions have not yet been addressed: (a) Regarding disruption starting time point, will earlier system disruption generate greater impact on network performance? (b) Regarding disruption duration, will longer-lasting disruption have a stronger impact? When is the critical period within the 24-h daily cycle? (c) Regarding spatial variation, which regions and HSR lines are more vulnerable? Regarding HSR stations, which ones should be given higher priorities to defend the overall network performance in certain time slots? (d) How does disruption propagation regimes influence network performance? Does the influence vary across time slots?

To answer these questions, this study focuses on investigating the spatiotemporal characteristics of HSR network performance with exogenous disturbances, especially the cascading failures. We examine the robustness of the HSR network affected by disruptions at different times of a day or different regions. This study proposes a new framework to analyze the cascading failures of nodes in the HSR network considering different disruption time slots and different affecting regions and different stations in the HSR network. Firstly, a weighted directed HSR network is built according to the service timetable, in which an attribution matrix for each node and edge, including the service ID, departure/ arrival station name, and departure/arrival time is incorporated. Secondly, a new algorithm is built to perform the robustness assessment considering the disruption time slots, by removing records associated with disrupted nodes from the attribute tables according to the service departure time and arrival times. The weighted network efficiency considering both travel time and service frequency along the shortest topological path is built to measure the network performance. Three types of disruption propagation regimes, the random, malicious, and event-led regimes, are analyzed, where HSR stations are disrupted one-by-one in different sequences. Lastly, taking China as a case study, the robustness of the weighted HSR network is investigated from both time- and space-dynamic perspectives.

This study contributes to the existing literature in several ways. Firstly, a new framework is proposed to analyze the cascading failures of nodes in the HSR network considering different times of the day and different affecting regions. Previous studies normally assess the railway network robustness in a static manner and do not differentiate disruptions happen in different time slots. The assessment is conducted by completely removing the disrupted nodes and/or connecting edges (Lordan and Albareda-Sambola, 2019; Hong et al., 2019; Li and Rong, 2020). This method cannot identify the impacts of cascading failures of nodes that happen in different time slots. Motivated by this, we propose a holistic framework to incorporate temporal heterogeneity in the robustness assessment. In the proposed framework, the HSR service network is updated dynamically according to the disruption propagation evolution and the HSR service timetable. Specifically, within a given time slot, an HSR service is considered as disrupted (and removed from the network) if and only if the disruption start time precedes the HSR departure/arrival time. The affected nodes/edges are taken out of the service network only in the time slots where the disruption is present. Once the service resumes, the network is updated accordingly. The proposed framework enables dynamical assessments of the HSR service network performance and robustness.

Secondly, we measure the integrated network efficiency on account of travel time, frequency, and network topology. Empirical evidence has documented a number of factors that travelers may consider when they take public transportation services, among which the shortest travel time, service frequency, and shortest topological path (number of transfers) are the key factors (e.g., Tillema et al., 2010). The three factors respectively reflect the topology-based, the service-based, and the locational-based characteristics of a service network and are all key determinants of travelers' route choice. In general, travelers prefer routes with fewer transfers, shorter travel time, and higher frequency (more flexible departure time choices). We find that most previous studies of railway network efficiency considered part of the key factors while missing consideration of other aspects of the network efficiency. In this study, a composite

[1] For example, influenced by the Typhoon Lekima, the HSR services between Shanghai and other cities in China were temporarily shut down in a whole day at August 9, 2019 (https://www.jiemian.com/article/3389622.html, accessed: September 15th, 2019); while influenced by the strong wind causing foreign matters hanging on the contact network between Tai'an and Qufu, several services on Beijing -Shanghai HSR line were delayed about one hour during 13:02 to 14:06 on October 25, 2019 (http://m.zhicheng.com/news/xwyd/n/298840.html, accessed: October 25th, 2019).

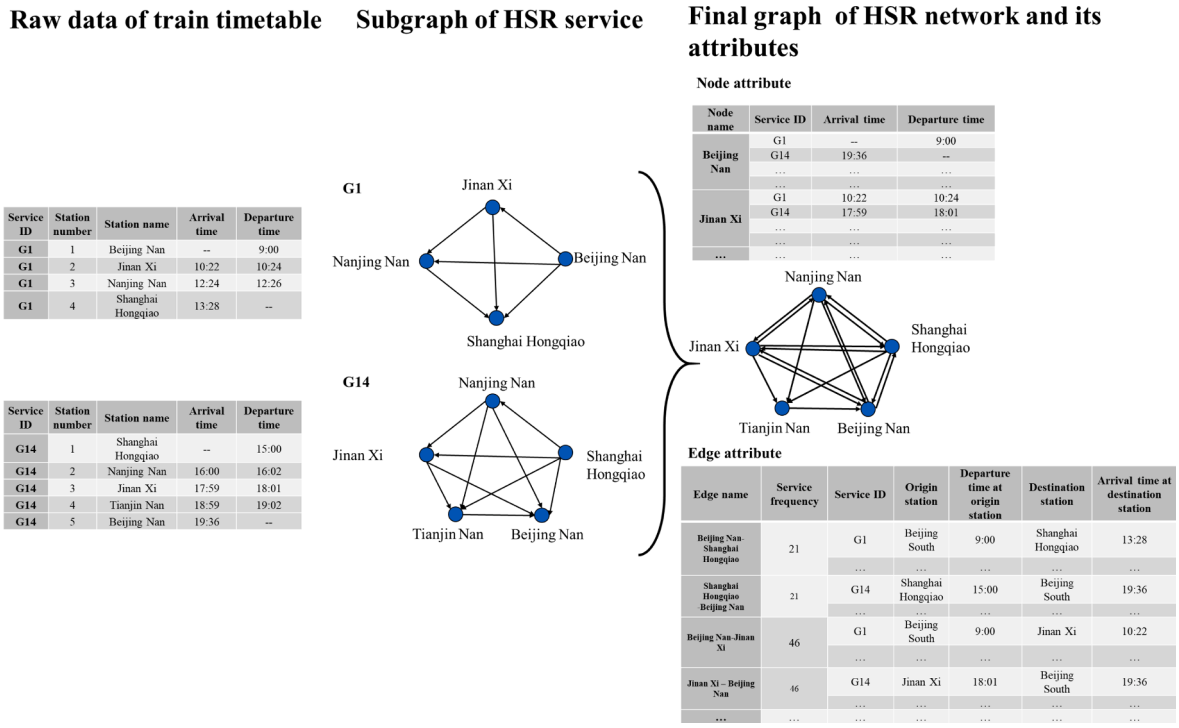

Service ID	Station number	Station name	Arrival time	Departure time
G1	1	Beijing Nan	--	9:00
G1	2	Jinan Xi	10:22	10:24
G1	3	Nanjing Nan	12:24	12:26
G1	4	Shanghai Hongqiao	13:28	--

Service ID	Station number	Station name	Arrival time	Departure time
G14	1	Shanghai Hongqiao	--	15:00
G14	2	Nanjing Nan	16:00	16:02
G14	3	Jinan Xi	17:59	18:01
G14	4	Tianjin Nan	18:59	19:02
G14	5	Beijing Nan	19:36	--

Node name	Service ID	Arrival time	Departure time
Beijing Nan	G1	--	9:00
	G14	19:36	--
	…	…	…
Jinan Xi	G1	10:22	10:24
	G14	17:59	18:01
	…	…	…
…	…	…	…

Edge name	Service frequency	Service ID	Origin station	Departure time at origin station	Destination station	Arrival time at destination station
Beijing Nan-Shanghai Hongqiao	21	G1	Beijing South	9:00	Shanghai Hongqiao	13:28
		…	…	…	…	…
Shanghai Hongqiao Beijing Nan	21	G14	Shanghai Hongqiao	15:00	Beijing South	19:36
		…	…	…	…	…
Beijing Nan-Jinan Xi	46	G1	Beijing South	9:00	Jinan Xi	10:22
		…	…	…	…	…
Jinan Xi – Beijing Nan	46	G14	Jinan Xi	18:01	Beijing South	19:36
		…	…	…	…	…
…	…	…	…	…	…	…

Fig. 1. The modeling process of HSR network of G1 and G14 services.

indicator, namely the weighted network efficiency, is built to incorporate all three factors into the evaluation metric of network efficiency, aiming to provide a comprehensive appraisal framework for HSR network efficiency.

Thirdly, the variation of the robustness of the HSR network in China is assessed in spatial and temporal dimensions. In the space dimension, we examine the impact of node disruptions in different geographical regions, along different HSR corridors or a certain HSR station. In the time dimension, we examine the impact by simulating 576 (24 × 24) disruption propagation scenarios, each corresponding to a specific time slot of disruption occurrence. It is often the case that nodal disruptions only affect a certain period or a certain realm of space. Several studies began to explore the spatiotemporal vulnerability of the HSR system in China, but they mainly focused on selected stations or disruptions that affect a small realm of space (e.g., Hong et al., 2019; Li and Rong, 2020). In this study, we explore the impacts of nodal cascading failures on the performance of the overall HSR network. By examining the evolutions of weighted network efficiency in different scenarios, we find that service disruptions starting at 10:00; lasting for a longer duration, especially that during 10:00–15:00; affecting the HSR stations in East China and Yangtze River Delta regions; or along the Harbin-Hong Kong corridor have the largest impact on overall network performance. The most critical stations are mostly located at the intersections of multiple HSR lines, which include Guangzhou South, Nanjing South, Chengdu East, Hankou (a station in Wuhan City), Shijiazhuang, Xi'an North, Wuhan, and Zhengzhou East stations. For example, Wuhan City is located near the geographical center of Mainland China and lies on the intersection of several major HSR lines. Although the number of HSR stations in Wuhan City accounts for 1.6% of that in China, the suspension of Wuhan's HSR stations can generate a larger impact on the overall performance of the national HSR network than the other cities (i.e. Guangzhou, Shanghai, and Nanjing).

Finally, the robustness of the HSR network under three types of disruption propagation regimes is considered to illustrate different scenarios where disruptions spread in the HSR network in different sequences. The results show that the HSR network is the most resilient in the random propagation regime, where the disruption develops in a random sequence within the network. The HSR network is least robust to the betweenness-based propagation regime, where the disruption propagates from HSR stations with the largest betweenness centrality to the smallest. The robustness under degree-based and betweenness-based regimes depends mostly on the top 10% HSR stations, but that under random regime depends on 80% of the HSR stations. The impact of lockdowns during the COVID-19 outbreak in early 2020 is examined as a case study of the event-led disruption.

The remainder of the study is organized as follows. Section 2 describes the network description of the methodology; Section 3 and Section 4 present robustness assessment results with spatially and temporally variant disruptions, respectively; Section 5 discusses the impact of disruption propagation regimes; Section 6 concludes the study.

2. Network description and methodology

2.1. Network description

The railway network is widely characterized by two types of topology using train timetables and physical network attributes. One type is the so-called 'Space-L' topology, which defines HSR stations as nodes and connections/links between two adjacent stations on an HSR service[2] route as edges (Sienkiewicz and Hołyst, 2005). The other type is the 'Space-P' topology, which is a more general network. Space-P defines HSR stations as nodes; differently, edges are defined for all links between all station pairs along the HSR line (Zhang et al., 2013). For example, Station A and B are not immediate neighbors and they are served by the same HSR service. In this case, there is a link defined between A and B in Space-P topology, but no link can be defined in Space-L topology. In this sense, Space-P has a more decent generalization ability by ignoring the sequential order of stops along a route (Zhu et al., 2008), which can thus better describe the accessibility and convenience of the transportation network (De Bona et al., 2016). We utilize the Space-P topology to construct the HSR network in this study. Fig. 1 shows an example of the network construction process from the train timetable data to the weighted HSR network associated with two HSR lines.

In the Space-P of HSR network, a node represents an HSR station. Any ordered node-pair is linked by an edge if there is an HSR service operating between this ordered node-pair, and the weight of each link is the service frequency between the ordered node-pair. On this basis, the topological structure of HSR network is characterized by a weighted directed multigraph[3] $G= (V, E, W, VA, EA)$, where G denotes the HSR service network in China, V is the station set, represented by $V=\{v_i: i = 1,2,\ldots,n\}$, where v_i represents node i, n is the number of nodes (HSR stations); the edge set ($E=\{e_{ij}: i = 1,2,\ldots,n\}$) is the ordered node-pairs with HSR services running directly from node v_i and v_j; and the weight set $W=\{w_{ij}: i,j = 1,2,\ldots,n\}$ is a set of edge weights, which is defined by the service frequency running directly from node v_i and v_j. VA refers to the attribution matrix of each node, including the basic information of all HSR services stopping at it, i.e., the service ID, station name, departure time, and arrival time; EA is the attribution matrix of each edge including all the basic information of HSR services between two nodes, i.e., the service ID, station name of origin node, departure time of origin node, station name of the destination node, and arrival time of destination node.

2.2. Network efficiency metric

Considering most travelers prefer routes with fewer transfers, shorter travel time, and more service choices (represented by service frequency), each directed edge is weighted by both service frequency and actual travel time calculated according to the train timetable along the directed edges in our study. The travel distance from origin node i to destination node j weighted by service frequency and actual travel time is calculated, to respectively reflect how connected and accessible the origin node i is to destination node j in the network. In this way, the network efficiency weighted by service frequency and travel time, namely the *Weighted Network Efficiency (WNE)*, is proposed. It is a composite index, which measures the inverse product of the sum of reciprocal service frequencies and the shortest travel time with the prerequisite of least transfers through the shortest topological path. It is written as:

$$WNE = \frac{2}{n(n-1)} \sum_{i,j=1(i\neq j)}^{n} 1/\sqrt{W_{ij} \times T_{ij}} \tag{1}$$

where WNE is the weighted network efficiency metric of the network; T_{ij} is the travel distance measured by the travel time from origin node i to destination node j; W_{ij} is the travel distance weighted by the service frequency from origin node i to destination node j. The product of W_{ij} and T_{ij} represents the generalized travel distance weighted by both service frequency and journey time, where frequency and time have equal weight in the measurement. This reflects the travel behavior that travelers will consider both the journey time and service frequency (size of selection choice set) when making travel choices. The equal weight implies that the changes of both distance measures have equal impact magnitude on the overall perception of travel distance between the origin–destination pair.

Following the previous study by Zhou et al. (2019), the travel distance weighted by service frequency from origin node i to destination node j along the shortest topological path is calculated by:

$$W_{ij} = \min_{p\in P_{ij}} \sum_{k\in p} \frac{1}{w_k} \tag{2}$$

whereW_{ij} denotes the travel distance weighted by service frequency from origin node i to destination node j, which equals the minimum sum of inverse service frequency on each edge of the shortest route between the two nodes. This variable represents the travel distance weighted by inverse service frequency, based on the shortest topological path. It refers to the 'effective' travel distance rather than the 'geographic' distance. In general, an origin–destination pair that requires more transfers or has less frequent services will be perceived less accessible, and thus the 'effective' distance decreases with frequency.

[2] The high-speed train (HST) refers to the rolling stock (a set of railway vehicles) that can be operated with a high-speed (over 200km/h); while the high-speed rail service (HSR service) refers to the high-speed passenger-carrying service with the G/D/C prefix, which is operated to a specific schedule.

[3] A multigraph is a graph which is permitted to have multiple edges (also called parallel edges).

In Eq. (2), P_{ij} represents the set of paths with the shortest topological path length (the least number of transfers) linking the origin node i and destination node j. A particular path p in P_{ij} consists of a series of directed edges k that form the shortest topological path (Liu et al., 2020). w_k is the weight of directed edge k, which is set as the HSR service frequency operating on the directed edge k. An origin–destination pair that requires more transfers or has less frequent services corresponds to a larger W_{ij} value, indicating that this route is less connected by HSR service.

The travel distance weighted by the travel time from origin node i to j in the condition of least transfers is defined as:

$$T_{ij} = \min_{i \neq j \in n, p \in P_{ij}, k, f \in p} (t_{jp}^{Arrivaltime} - t_{ip}^{Departuretime}) \tag{3}$$

where T_{ij} is the shortest travel time from the origin node i to destination node j, reflecting the travel distance weighted by travel time, and the larger value of T_{ij} indicating the less accessible from node i to node j;$t_{jp}^{Arrivaltime}$ and $t_{ip}^{Departuretime}$ are the arrival time at node j and departure time at node i along path p, respectively. Edges k and f can be represented by $\langle v_{origin}^{k}, v_{destination}^{k} \rangle$, $\langle v_{origin}^{f}, v_{destination}^{f} \rangle$,$v_{origin}^{k}$, $v_{destination}^{k}$, v_{origin}^{f}, $v_{destination}^{f} \in V$. When the edges k and f are connected, donated by $v_{destination}^{k} = v_{origin}^{f}$, the departure time at node v_{origin}^{f} should be an hour later than the arrival time at node$v_{destination}^{k}$.

The prerequisite of least transfers is imposed on the measurements of travel distances because most travelers prefer routes with fewer transfers to avoid inconvenience, transfer delay, and travel time uncertainty. When we search for feasible paths according to the service timetable, the 60-minute transfer duration requirement is enforced. For example, when there is no direct HSR service from node i to node j, meaning that travelers need to transfer to other HSR services via intermediate HSR stations, a feasible path requires that the departure time of the subsequent train at the interchange HSR station is at least 60 min later than the arrival time of the preceding train at intermediate HSR stations. On average, 60 min is sufficient and necessary for a traveler to transfer between services in the same station. In most cases, the travel distance considering the transfers is larger than that without such consideration.

According to the definition of robustness, the ability to retain its performance under disruptions and attacks, the percentage change in *WNE* (*DWNE*) is introduced to evaluate the robustness of the HSR network in this study. The percentage change of *WNE* measures the changing rate of *WNE* before and after the service disruption, which is the ratio of the gap between the *WNE* before and after the failures to the *WNE* before failures. The *WNE* before failures is the *WNE* of the initial graph, which is the graph without disruptions. The formula of *DWNE* is given by:

$$DWNE = \frac{(WNE_{before} - WNE_{after})}{WNE_{before}} \times 100\% \tag{4}$$

where *DWNE* is the percentage decrease of *WNE* before and after the failures; WNE_{before} and WNE_{after} are the *WNE* before and after failures, respectively. While the network efficiency metric, *WNE*, can take any value without a specific range; the robustness metric, *DWNE* (the percentage decrease of WNE), ranges between 0 and 100%. The larger the *DWNE* value is, the larger influence HSR failures will have on network efficiency, indicating the HSR network is less robust to disruptions.

To examine the effectiveness of the proposed metric, we compared the results measured by *DWNE* and several other metrics adopted by previous studies, including the weighted network efficiency (based on Zhou et al., 2019′s definition), the average shortest travel time with least transfers (Hong et al., 2019), the network efficiency (Chen et al., 2020), the number of affected trains, and the influenced passengers based on expected demand. The details are presented in Appendix A.

2.3. Robustness assessment procedure

It is often the case that HSR disruptions only affect a certain period or a certain realm of space. In this study, we propose a new algorithm to assess the network robustness with respect to service disruptions that occur in varying time slots (differentiated by the disruption start time and duration) and in varying locations (differentiated by geographical divisions and HSR corridors). The service disruption of an HSR station in a certain time slot means that HSR service may be suspended at the affected station for a certain time slot instead of a whole day. Therefore, we examine the time-varying robustness by removing the records in the attribute table of edges according to the departure time or arrival time at the failure node, instead of removing the edges connected to the failure node. The space-varying robustness is mostly explored by assessing the impacts of individual station failure and the spatially local failure (Hong et al., 2019) or the disruptions occur at a few major HSR stations (Li and Rong, 2020); however, less attention has been paid to the disruption of all stations in the network.

Without loss of generality, we consider 576 (24 × 24) different time slots, each representing a combination of a particular disruption start time (denoted by $a \in A$) and a disruption duration (denoted by $b \in B$). Set A represents the set of disruption start times and set$B$ represents the set of disruption durations. The disruption start time is set in line with the operating period of HSR service, between 00:00 and 23:00. For simplicity, the time resolution is set to be 1 h. Thus, the possible disruption start time $a \in A$includes 0:00, 1:00, …, 23:00. The disruption duration $b \in B$ can take any integer value between 1 h and 24 h. Each combination (a, b) is denoted by $A \times B = \{(a, b) | a \in A, b \in B\}$. Each combination is referred to as a disruption time slot, or a simulation scenario thereafter.

The failure of the HSR system in the real world may come in different types, such as station failure, track failure, and rolling stock failure. The impact of HSR failure varies as they may be caused by different reasons. Considering the broad scope, it is difficult (if not impossible) to cover all types. In this paper, we consider a typical type of HSR station failure that only affects the train services that were scheduled to arrive at/depart from the stations. The services passing by the station will not be affected as long as other stations

Table 1
Algorithm for robustness assessment considering failure time slots.

Algorithm1: Robustness assessment
Input: The initial graph G^0; the disruption propagation regimes S. **Output:** WNE^S, $DWNE^S$ 1: Randomly select a time slot A ▷Step 1 2: $e^0 \leftarrow$ Compute Graph Efficiency in the initial graph G^0, and $WNE^S = \{e^0\}$ ▷Step 2 3: **for** each strategy s in S do. ▷Enumerate the propagation regimes 4: **while** G is not paralyzed or all nodes have been attacked **do** 5: $n \leftarrow$ Select failure node according to the regime (s) ▷Step 3 6: $G \leftarrow$ Modify the attribute of edges connected the failure node ▷Step 4 7: $e \leftarrow$ Compute graph efficiency(G) ▷Step 5 $d \leftarrow$ Compute changes in graph efficiency(G) 8: Add e to WNE^s Add d to $DWNE^s$ 9: **Return** WNE^S, $DWNE^s$

along the line remain operating. This is very realistic. For example, during the early stage of lockdown due to the COVID-19 outbreak, the HSR stations in Wuhan City were closed but some services remain operation without stopping in Wuhan. To contextualize the analysis, several related assumptions are introduced.

In each scenario, we consider that the HSR disruption occurs at specific HSR stations in specific time slot(s) such that only the HSR services that were scheduled to arrive at/depart from these stations during these time slots will be suspended. Other HSR services will not be affected. This is realistic as China's HSR stations commonly have one (or more) track(s) is/are designated for passing-by services. In contrast with other tracks that are used for arrival/departure services, these tracks do not serve for passenger boarding and thus do not have platforms. Therefore, in the circumstances of station disruption/closure, it is often the case that the passing-by track (s) can still be useable.

Regarding the propagation of disruption in the HSR network, we consider the case where HSR stations fail in batches in successive time steps; stations of the same batch are assumed to be disrupted at the beginning of the time step. To simplify the analysis, there is no further subdivision in each time step. The model can be readily extended to cases with further discretized time slots.

As noted in the Introduction, HSR stations may face different types of disturbances such as natural hazards, technical failures, man-made failures (e.g. cyber-attack), and disruptions caused by social/public health events. In particular, natural hazards, such as extreme weather, are more likely to disrupt nodes randomly. Malicious attacks, including disruptions caused by political events and terrorist attacks, are more likely to target important HSR stations (Chen et al., 2020). Technical failures also have larger probabilities occurring at stations with larger traffic volume and service frequency. Social/public health event-led disruption, such as that caused by the outbreak of COVID-19 in early 2020, may disrupt a series of HSR stations in a particular sequence, which is driven by the nature of the event. The above propagation regimes cover various types of disruptions in the real world and thus are considered to be representative.

Thus, in this study, three types of disruption propagation regimes are considered to mimic different situations where disruptions spread in the network, i.e., random, and malicious and event-led propagation regimes. The random propagation regime refers to the situation where HSR stations are disrupted one-by-one in a random sequence. The malicious propagation regimes refer to the situation where HSR stations are disrupted in a descending sequence according to the status of nodes in the initial and upgraded graph. The malicious propagation regime refers to the situation where HSR stations are disrupted in a descending sequence according to the status of nodes in the initial and upgraded graph. The nodes with the highest status in the initial graph fail firstly, which results in the changes in the edge weight connected it, and then the nodes with the highest status in the remaining network are disrupted until all the nodes fail or when the network has isolated nodes only. Under the event-led regime, the sequence of station disruption occurrence depends on the spread of the event (e.g., lockdown sequence during the COVID-19 outbreak).

Table 1 presents the algorithm we use to perform the robustness assessment. The input of the algorithm is the HSR network attributes introduced in Section 2.1 and the output is a set of *Weighted Network Efficiency* (*WNE*) and *Decrease in Weighted Network Efficiency* (*DWNE*) metrics, which are defined in Section 2.2. The detailed procedure of robustness assessment considering disruption time slots is as follows:

Step 1: Randomly choose a time slot of service disruption by deciding the start time of disruption and disruption duration.

Step 2: Calculate the *WNE* of the initial graph.

Step 3: Choose the failure node among the node-set based on the given disruption propagation regime.

Step 4: Find out the edges associated with the affected node according to the departure time or arrival time at the node from the attribute table, i.e., if the departure time or arrival time at the failure node is within the duration of the system failure.

Step 5: Recalculate the weight of each edge, and the *WNE* and *DWNE* of the updated network; and if there is more than one subgraph, the weighted network efficiency is calculated based on the maximal connected subgraph.

Step 6: Repeat steps 3, 4, and 5 until the network has isolated nodes only or until all nodes are crashed.

2.4. Case study settings

Taking the HSR network of China as a case study, the robustness of the HSR network is explored in time- and spatial-dynamic dimensions.

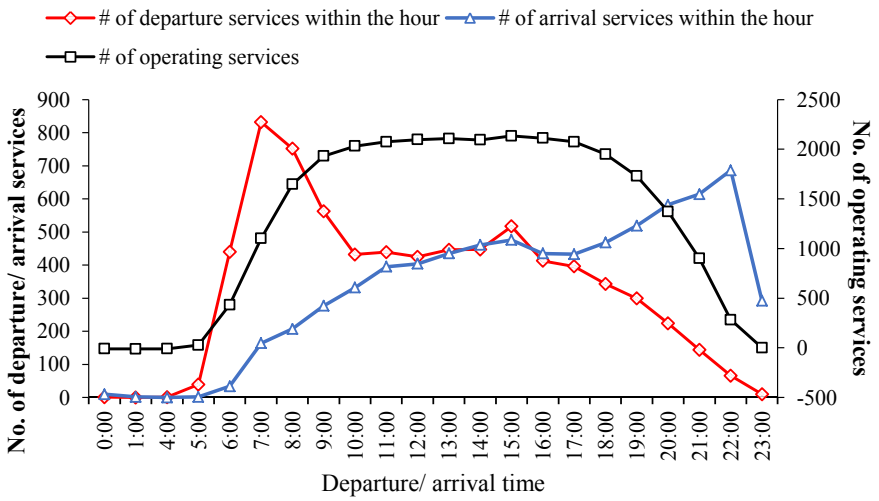

Fig. 2. Daily frequency of departure/arrival/operating HSR services over time.

2.4.1. Data processing

High-speed railway in China includes the railway lines newly built for dedicated passenger services with the operating speed over 250 km/h and the upgraded railway lines for passenger services with the operating speed over 200 km/h according to the '*Railway Safety Management Regulations*' published by the central government of China. According to this definition, HSR services include all train services operating on HSR lines, including the G prefix HSR services (running on newly-built HSR lines), D prefix HSR services (running on upgraded HSR lines), and C prefix HSR services (running on intercity HSR lines). The study areas include all the railway stations located in mainland China (excluding Hong Kong and Taiwan) with the G, D, C prefix HSR services. Up to 31 December 2019, 5,962 HSR services are operating on more than 35,000 km HSR lines and 1061 HSR stations in mainland China, according to the data collected from the China Railway website (https://www.12306.cn/index/) and the website of Huochepiao (http://huochepiao.com/). The collected data contains service ID, station name, departure time, and arrival time at each station. The longitude and latitude of each station are collected using Baidu API (http://api.map.baidu.com/lbsapi/getpoint/index.html).

2.4.2. Statistical characteristics of China's HSR network

Fig. 2 illustrates the distribution of departure HSR services, arrival HSR services, and operating HSR services, which reflects the temporal distribution of HSR services. Taking an hour as the study unit, we calculate the number of HSR services departing, arriving, or remaining in the network to understand the supply characteristics of HSR services in China. In Fig. 2, data points on the black curve represent the number of operating services at the particular time point (for example at 9:00), which accounts for the number of services remaining in the network. This is calculated by the difference between accumulated departure and accumulated arrival services (e.g., the difference between departure accumulation and arrival accumulation during 5:00–9:00). For the other two curves, each data point on the red curve represents the number of departure services within the 1-hour period, e.g., the data point for 9:00 represents the departure services between 9:00–10:00. Similarly, each data point on the blue curve represents the number of arrival services within the 1-hour period.

The temporal distribution of departure HSR services and arrival HSR services differs significantly. The peak of departure HSR services arises between 7:00 and 8:00. The number of HSR services reaches 832 during this period, accounting for 11.51% of the total number of HSR services per day. The number of departure HSR services dramatically decreases to 432 between 10:00 and 11:00, then keeps steady between 430 and 450 till 15:00, gets a second peak at 517 between 15:00 and 16:00, and then decreases slowly till 24:00. Before the peak between 22:00 and 23:00, the number of arrival HSR services increases slowly and continuously from 5:00 to 22:00. In terms of the operating HSR services, the number increases dramatically from 5:00 to 11:00 with the value increased from 27 to 2031, keeps at 1950–2150 till 19:00, and then decreases dramatically to 0 till 24:00. Before 9:00, the number of operating HSR services is greater than that of the arrival HSR services, but less than that of departure HSR services; During 9:00 and 20:00, the number of operating HSR services is greater than both of the departure and arrival HSR services. After 20:00, the number of operating HSR services is less than that of the arrival HSR services, but greater than that of departure HSR services. This indicates that most HSR services are operated between 9:00 and 20:00, and less than 10 HSR services are operating between 0:00 am and 5:00.

3. The HSR network robustness with spatially variant disruptions

HSR stations in different regions might be influenced by different types of natural hazards, i.e. those in East and South China are more likely to be attacked by typhoons, and those in North China might be influenced by heavy snows. Technological failures are more likely to influence the stations along certain HSR lines, instead of the whole network. Additionally, man-made disruption might happen anywhere, even in one city or one station. Triggered by this, we examine the network performance when the system experiences

disruptions in certain regions, lines, or a certain HSR station to understand the robustness of the HSR network affected by spatially variant disruption incidents. Taking HSR stations in Wuhan City and Hubei Province as a case study, the influence of COVID-19 on the network performance is examined and compared with several transportation hub cities[4] in China. In this section, we focus on the effect of spatial variation. The disruption time slot is assumed to be a whole day.

Table 2 summarizes the HSR service network characteristics and robustness metrics in different geographical divisions, along HSR corridors, in Hubei Province, in Wuhan City, and in other transportation hubs cities, respectively. The metrics include the number of HSR stations, the average degree, and the decrease of *WNE* when all nodes are disrupted in the geographical divisions and along HSR corridors in a whole day. Amongst, the geographical divisions are divided according to the geographical location and natural condition, which include the East, South, Northwest, Northeast, Southwest, Central and North China (a total of 7 geographical divisions); the HSR corridors are defined according to the "Medium- and long-term railway network planning (revised in 2016)", which proposed that China will build eight vertical- and eight horizontal-HSR corridors by 2030. By the end of 2019, there are 11 HSR corridors with through or several segments in operation.

The results show that the HSR disruption occurs in East China generates the largest influence on network performance, followed by that in Central China, North China, and South China. Specifically, the node disruption in East China might lead to a 52.04% decrease in *WNE*, indicating that more than half of network performance is failed. The percentage is 34.66% for Central China, 25.9% for North China, 25.63% for South China, 22.99% for Southwest China, and 21.95% for Northwest China, respectively. The disruption has the smallest impact on *WNE* in Northwest China (11.23% decrease). The reason might be that the number of HSR stations and the average number of adjacencies are the largest in East China and the smallest in Northwest China.

The node disruption of the Harbin-Hong Kong passageway generates the largest influence on the network performance across all HSR corridors. The *WNE* decreased by 68.36% if the Harbin-Hong Kong corridor stopped working, followed by the Yangtze River (58.87%), Shanghai-Kunming (53.57%), and Coastal (51.96%) passageways. Except for the Harbin-Hong Kong passageway, the other three passageways all go through the city of Shanghai and several other major cities in the Yangtze River Delta, one of the most developed regions in China. The disruptions occur in Beijing-Lanzhou, Xiamen-Chongqing, Suifenhe-Manzhouli, and Hohhot-Nanning passageways have relatively smaller influences on network performance. The reason might be that some segments of these HSR corridors are still in the development stage which has not yet formed a well-connected network.

Our simulation also shows that the station suspension in Wuhan City may generate a larger influence on the network performance than other cities of Hubei Province. There were 17 HSR stations in Wuhan City in 2019, only accounting for 1.6% of that in China. However, the disruption of these 1.6% HSR stations in a whole day may lead to a 14.33% decrease in the *WNE* of the overall HSR network. Compared with the other transportation hub cities, the *DWNE* caused by Wuhan HSR suspension is the largest, followed by Guangzhou, Shenyang, Zhengzhou, Nanjing, Shanghai, Chengdu, Lanzhou, and Beijing. The reason might be that Wuhan City is located near the geographical center of Mainland China and the intersection of several HSR lines, i.e. Beijing-Guangzhou HSR line, Wuhan-Jiujiang HSR line, Shanghai-Chengdu HSR line, Wuhan-Huangshi and Wuhan-Huanggang intercity railways. It is interesting to find that suspension of Beijing's HSR stations is corresponding to the smallest *DWNE*, indicating the largest robustness among the concerned transportation hubs. The reason might be that the HSR stations in Beijing serve different HSR lines in different directions[5], leading to relatively larger path length (more transfer delay) traversing Beijing than the other cities. In the circumstance of HSR station disruption in Beijing, passengers can transfer service at other nearby HSR stations, e.g., HSR stations in Tianjin or Shijiazhuang, without too much additional cost. The journey time from Beijing to Tianjin or Shijiazhuang by HSR service is 0.5 and 1.15 h(s), respectively. Most Beijing services stop at Tianjin or Shijiazhuang.

There were 64 HSR stations in Hubei Province in 2019 and the disruption of these HSR stations can lead to a 16.73% decrease in the *WNE*, which is slightly greater than that caused by Wuhan City. The reason might be that most HSR stations in other cities of Hubei Province are connected with Wuhan City. Once the HSR stations in Wuhan City are disrupted, the network connectivity of HSR stations is largely affected. The results imply that HSR stations in Wuhan City play an important role in the national HSR network, but a dominating role in Hubei Province.

Fig. 3 presents the distribution of the decrease in *WNE* when a single HSR station stops working for the whole day in China. The HSR stations that can cause a large drop in *WNE* are mainly located at the intersection of several HSR lines or the Yangtze River Delta. Specifically, there are 16 HSR stations associated with a decrease in *WNE* greater than 0.66% (marked by the red dot in Fig. 3). This percentage is equivalent to 2.5 standard deviations (σ) plus the mean value (μ) of the *WNE* decrease associated with all HSR stations in China. We find that all these top stations are located at intersections of trunk HSR lines. There is a total of 81 HSR stations that can cause a decrease in W*NE* by 0.3%-0.66% ($\mu + 0.5\sigma$, $\mu + 2.5\sigma$). These stations are marked by yellow and orange dots in Fig. 3. They are distributed mainly in the Yangtze River Delta and the Pearl River Delta; several of them are located on the intersection of trunk HSR lines or inter-city HSR lines. Overall, the HSR stations where a single station disruption can lead to a decrease in *WNE* larger than the national mean (0.3%) are mainly located at the intersections of HSR lines or in the developed areas of China, i.e., Yangtze River Delta and Pearl River Delta.

We further examine the scenarios where one particular HSR station is disrupted by incidents that start at different times or last for different durations, respectively. Based on the decrease in *WNE* associated with each HSR station disruption, we identify the top 10

[4] Our analysis includes Beijing, Shanghai, Nanjing, Guangzhou, Chengdu, Lanzhou, Zhengzhou and Shenyang. All of them are the comprehensive rail hubs according to the national "Medium- and long-term railway network planning (revised in 2016)".

[5] For example, Beijing South station mostly serves the Beijing-Shanghai HSR line, Beijing-Tianjin intercity railway and so on; while Beijing West station serves the Beijing-Guangzhou HSR lines, Beijing-Kunming HSR lines etc.

Table 2
HSR network characteristics and robustness metrics in different geographical divisions and along HSR corridors in China.

		No. of stations	Average degree	% of the decrease in WNE	Scope
National level		1061	75.6	100	All cities in China, excluding Hong Kong, Macao, and Taiwan
Geographical Divisions	East China	287	112.2	52.04	80 cities in Shanghai, Jiangsu, Zhejiang, Anhui, Jiangxi, Shandong, and Fujian Provinces
	South China	158	50.69	25.63	38 cities in Guangdong, Guangxi, and Hainan Provinces
	Northwest China	73	48.25	11.23	56 cities in Shaanxi, Gansu, Qinghai, Ningxia, Xinjiang, and the west of Inner Mongolia Provinces
	Northeast China	144	60.19	21.95	41 cities in Heilongjiang, Jilin, Liaoning, and east of Inner Mongolia Provinces
	Southwest China	159	57.03	22.99	56 cities in Chongqing, Sichuan, Guizhou, Yunnan, and Xizang Provinces
	Central China	153	80.74	34.66	44 cities in Henan, Hubei, and Hunan Provinces
	North China	87	73.44	25.9	29 cities in Beijing, Tianjin, Shanxi, Hebei, and the central region of Inner Mongolia Provinces
Eight Vertical Corridors	Coastal passageway	189	90.41	51.96	40 cities located along the HSR corridor along the eastern coast of China
	Beijing–Shanghai passageway	78	112.44	42.45	23 cities located along Beijing – Shanghai, Hefei-Bengbu, Hefei-Hangzhou, and Nanjing –Hangzhou HSR lines.
	Beijing–Hong Kong (Taipei) passageway	69	115.62	29.54	18 cities located along Shangqiu-Hefei-Hangzhou, Hefei-Fuzhou, Nanchang – Fuzhou HSR lines.
	Harbin–Hong Kong (Macau) Passageway	211	66.52	68.36	39 cities located along Harbin-Beijing, Beijing-Guangzhou, Guangzhou-Zhuhai, and Guangzhou-Shenzhen HSR lines.
	Hohhot–Nanning passageway	33	90.94	12.41	10 cities located along Zhengzhou-Jiaozuo, Loudi-Shaoyang, Hengyang-Liuzhou, and Nanning-Liuzhou HSR lines.
	Beijing–Kunming passageway	104	76.49	31.09	21 cities located along Beijing-Shijiazhuang, Shijiazhuang-Taiyuan, Beijing-Zhangjiakou, Datong-Xi'an, Xi'an-Chengdu, Chengdu-Chongqing HSR lines.
	Baotou (Yinchuan)–Hainan passageway	22	47.81	6.99	8 cities located along Hainan Roundabout Railway, Yinchuan-Wuzhong HSR line
	Lanzhou (Xining)–Guangzhou passageway	95	51.77	32.05	15 cities located along Chengdu-Guiyang, Guiyang-Guangzhou HSR lines
Eight Horizontal Corridors	Suifenhe–Manzhouli passageway	23	45.74	4.45	3 cities located along Mudanjiang-Suifenhe, Harbin-Mudanjiang HSR lines
	Beijing–Lanzhou passageway	12	42.42	3.02	5 cities located along Beijing- Hohhot HSR lines
	Qingdao–Yinchuan passageway	0	–	–	–
	Eurasia Continental Bridge passageway	69	84.8	18.87	22 cities located along Lanzhou-Lianyungang and Urumqi-Lanzhou HSR lines, except for Lianyungang and Xuzhou.
	Yangtze River passageway	139	74.77	58.87	22 cities located along Shanghai-Chengdu, Chengdu-Dazhou HSR lines.
	Shanghai–Kunming passageway	138	95.27	53.57	28 cities located along the Shanghai-Kunming HSR line.
	Xiamen–Chongqing passageway	19	94.47	4.15	4 cities located along Xiamen-Longyan, Longyan-Ganzhou HSR lines.
	Guangzhou–Kunming passageway	54	52.59	21.79	12 cities located along Nanning-Guangzhou, Nanjing-Kunming HSR lines.
Key regions affected by COVID-19	Hubei Province	64	64.75	16.73	13 cities in Hubei Province
	Wuhan City	17	51.82	14.33	The capital of Hubei Province and a comprehensive transportation hub
Key transportation hub cities	Beijing City	5	92.4	3.13	The capital of China and a comprehensive transportation hub
	Shanghai City	15	66.73	8.02	A comprehensive transportation hub
	Nanjing City	7	126.29	8.58	The capital of Jiangsu Province and a comprehensive transportation hub
	Guangzhou City	5	116.5	12.5	The capital of Guangdong Province and a comprehensive transportation hub
	Chengdu City	28	26.07	5.54	The capital of Sichuan Province and a comprehensive transportation hub
	Lanzhou City	7	40.71	5.43	The Capital of Gansu Province and a comprehensive transportation hub
	Zhengzhou City	8	98.13	8.69	The capital of Henan province and a comprehensive transportation hub
	Shenyang City	5	128.2	11.46	The capital of Liaoning province and a comprehensive transportation hub

Note: The degree of a node refers to the number of its adjacencies in a network (Freeman, 1978), defined by the number of nodes that are directly connected with the node and donated by k. The HSR stations located in the corridors are selected according to the cities they go through.

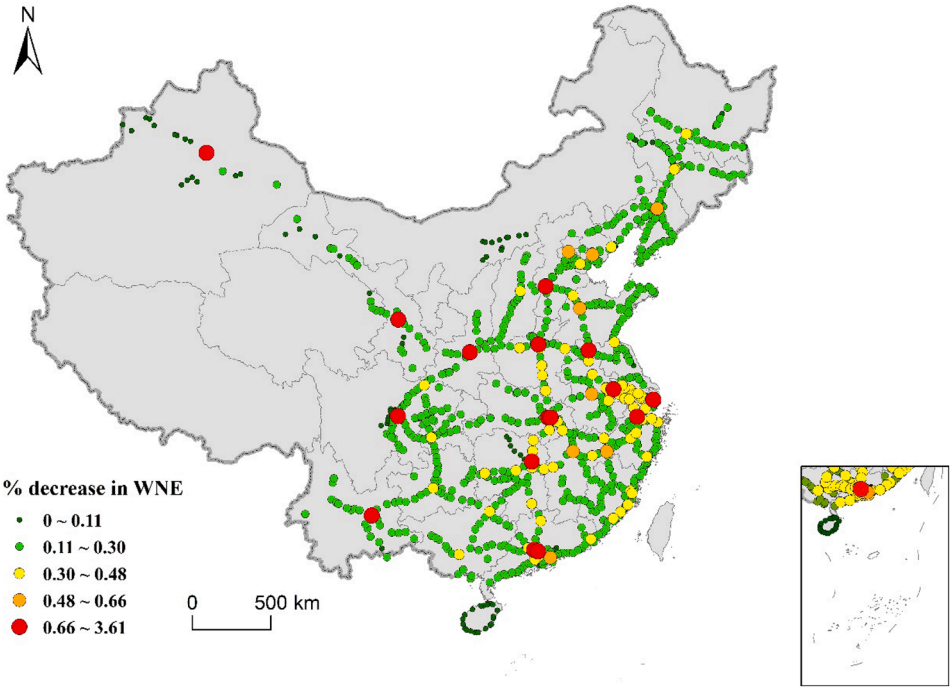

Fig. 3. Decrease in *WNE* when a single HSR station is disrupted for a whole day.

critical stations in various scenarios and summarize in Tables 3 and 4. Table 3 presents the decrease in *WNE* caused by disruption starting at 5:00, 7:00, 9:00, 11:00, 13:00, 15:00, 17:00, 19:00, and 21:00, respectively, where the disruption duration is fixed at 2 h. In Table 4, the disruption start time is fixed at 7:00, and the disruption duration is set to be ranging from 1 to 16 h.

The HSR stations with the top 10 decrease in *WNE* vary across different time slots (see Tables 3 and 4). There are only two HSR stations, namely Guangzhou South and Nanjing South, appearing in all the selected 17 time slots. Xi'an North, Hankou (a station in Wuhan City), Shijiazhuang, Chengdu East, Wuhan, Zhengzhou East and Changsha stations are all listed in the top 10 HSR stations in no less than 10 time slots among the 17 selected time slots. Some HSR stations are appearing at only one certain time slot or no more than 4 time slots. That's to say, all of these HSR stations have a substantial impact on the whole network in several certain time slots. For example, Shanghai Hongqiao HSR stations only appear in the top 10 HSR stations lists in the time slots of 5:00–7:00 and 9:00–11:00, and Nanjing HSR stations only appear in the time slot of 5:00–7:00. Overall, the Guangzhou South and Nanjing South are the critical stations for all the selected time slots, and Xi'an North, Hankou, Shijiazhuang, Chengdu East, Wuhan, Zhengzhou East, and Changsha HSR stations are the critical stations in the majority of time slots, while the other HSR stations in Tables 3 and 4 are the critical stations in several certain time slots or even one time slot. All the critical stations in all or the majority of the selected time slots are located at the interaction of serval HSR lines, i.e. Zhengzhou East located at the intersection of Beijing-Guangzhou and Longhai HSR lines, and Nanjing South located at the intersection of Beijing-Shanghai, Shanghai-Chengdu, Nanjing-Hangzhou, Ning'an, and Nanjing-Hefei HSR lines.

4. The HSR network robustness with temporally variant disruptions

This section examines the effects of disruption time slots on the network performance and identifies the critical time slots, at which the disruptions have the largest influence on network performance. To better understand the effects of disruption time slots on the network performance, we assume that all the HSR stations are simultaneously disrupted in the time slot.

We simulate disruptions that happen in 576 (24×24) different time slots (introduced in Section 2.3) and assess the robustness of the HSR network in each scenario. Fig. 4 illustrates the *WNE* of HSR networks in 576 time slots, reflecting the *WNE* when all nodes are disrupted in a certain time slot, where the *x*-axis represents the disruption start time, the *y*-axis represents the disruption duration, and *z*-axis shows the *WNE* when all nodes are disrupted in a certain time slot. Contours of *WNE* in the domain of disruption duration and disruption start time are shown by the color curves in the xy-plane. It can be seen that the earlier the disruption starts or the longer the disruption duration is, the larger impact the disruption has on the network performance. In the following subsections, we further analyze the changes in *WNE* with different disruption start times and durations.[6]

[6] In Figs. 4, 5, 6, 7, 8, the absolute values of Weighted Network Efficiency (*WNE*) are presented instead of the relative value *DWNE*. The purpose is to better illustrate the evolutions of network efficiency, while DWNE can be immediately obtained by comparing the *WNE* with a constant (i.e., the *WNE* of the initial graph, 0.07931).

Table 3
Top 10 stations in the HSR network with the largest *DWNE* with different disruption start times.

	5:00	7:00	9:00	11:00	13:00	15:00	17:00	19:00	21:00
1	Shanghai Hongqiao	Nanjing South	Nanjing South	Nanjing South	Guangzhou South	Guangzhou South	Xuzhou East	Nanjing South	Guangzhou South
2	Guangzhou South	Guangzhou South	Guangzhou South	Guangzhou South	Hankou	Nanjing South	Guangzhou South	Guangzhou South	Dingzhou
3	Shanghai South	Chengdu East	Xi'an North	Hankou	Kunming South	Lianyungang	Nanjing South	Chengdu East	Nanjing South
4	Nanjing South	Wuhan	Chengdu East	Xi'an North	Nanjing South	Hankou	Shenyang	Xi'an North	Shijiazhuang
5	Qingdao North	Lanzhou West	Shanghai Hongqiao	Wuhan	Xi'an North	Changsha South	Chengdu East	Hankou	Lanzhou West
6	Changchun	Hankou	Wuhan	Shijiazhuang	Wuhan	Wuhan	Zhengzhou East	Bozhou South	Zhengzhou East
7	Nanjing	Zhengzhou East	Hangzhou East	Zhengzhou East	Chengdu East	Shijiazhuang	Xi'an North	Fushun North	Shenzhen North
8	Zhengzhou East	Shijiazhuang	Shijiazhuang	Changsha South	Zhengzhou East	Xi'an North	Shijiazhuang	Caofeidian	Hankou
9	Shenzhen North	Xi'an North	Lanzhou West	Shenyang	Changsha South	Zhengzhou East	Changsha South	Wuhan	Xi'an North
10	Shenyang North	Bozhou South	Hankou	Chengdu East	Shijiazhuang	Chengdu East	Kaifeng	Hangzhou South	Minhe South

Table 4
Top 10 stations in the HSR network with the largest *DWNE* with different disruption duration.

	1 h	3 h	5 h	7 h	9 h	11 h	13 h	15 h
1	Nanjing South	Nanjing South	Nanjing South	Guangzhou South	Guangzhou South	Guangzhou South	Guangzhou South	Guangzhou South
2	Hankou	Guangzhou South	Guangzhou South	Nanjing South	Nanjing South	Nanjing South	Nanjing South	Nanjing South
3	Shijiazhuang	Chengdu East	Chengdu East	Chengdu East	Hankou	Hankou	Hankou	Xi'an North
4	Wuhan	Wuhan	Hankou	Hankou	Wuhan	Chengdu East	Chengdu East	Hankou
5	Guangzhou South	Lanzhou West	Wuhan	Xi'an North	Chengdu East	Wuhan	Xi'an North	Chengdu East
6	Zhengzhou East	Changsha South	Xi'an North	Wuhan	Xi'an North	Xi'an North	Wuhan	Zhengzhou East
7	Xi'an North	Shanghai Nan	Shijiazhuang	Zhengzhou East	Zhengzhou East	Zhengzhou East	Zhengzhou East	Wuhan
8	Chengdu East	Shijiazhuang	Zhengzhou East	Shijiazhuang	Shijiazhuang	Shijiazhuang	Shijiazhuang	Shijiazhuang
9	Changsha South	Xi'an North	Hangzhou East	Kunming Nan	Kunming South	Kunming South	Xuzhou East	Xuzhou East
10	Hangzhou East	Hankou	Lanzhou Xi	Changsha South	Changsha South	Changsha South	Changsha South	Urumqi

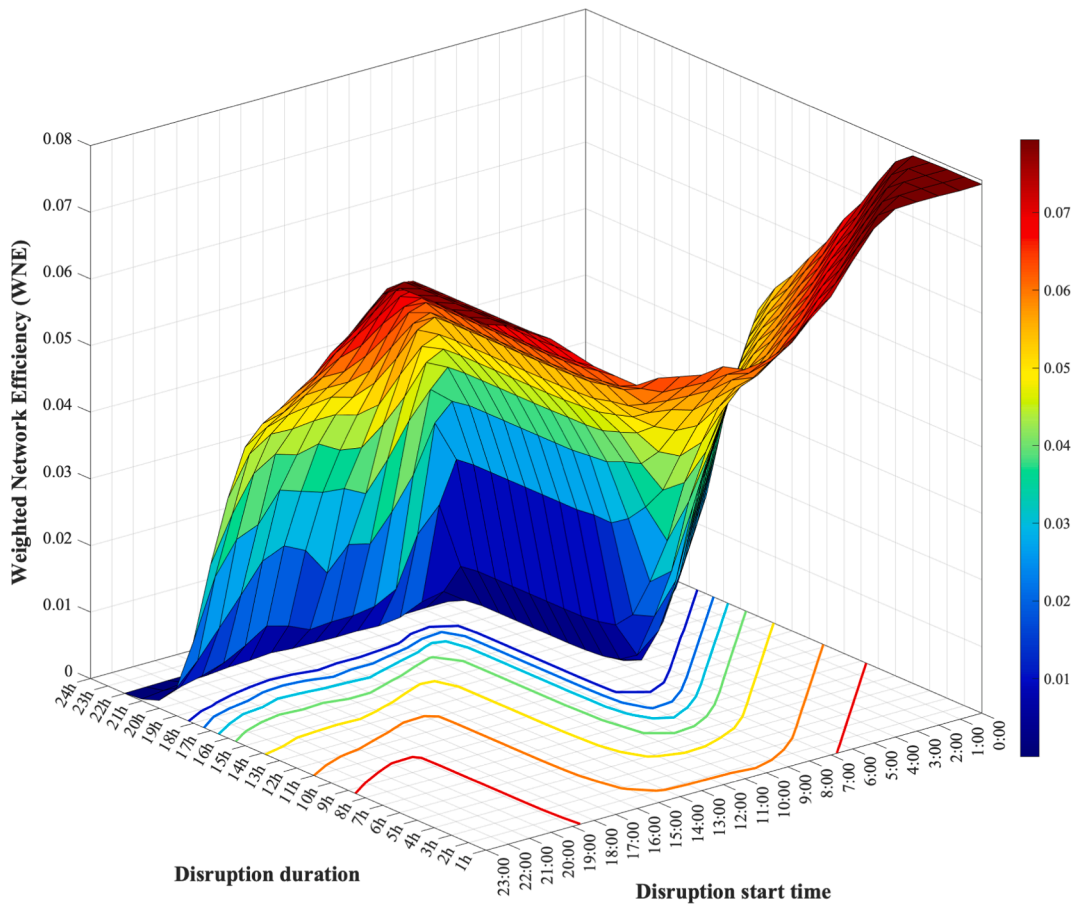

Fig. 4. Three-dimensional surface plot of weighted network efficiency, failure disruption start time and duration.

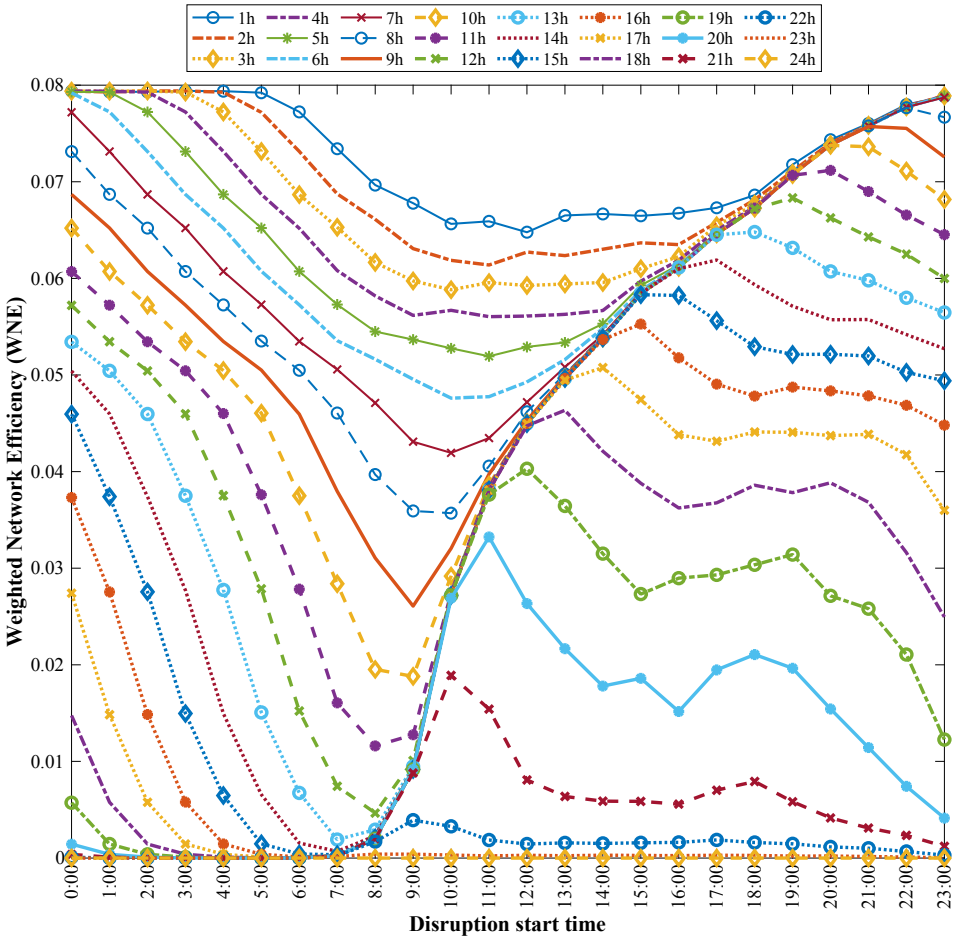

Fig. 5. The weighted network efficiency (*WNE*) with different disruption start times.

4.1. *Effect of the disruption start time*

Fig. 5 shows the relationship between *WNE* when all nodes are disrupted in a certain time slot and disruption start time. Each curve represents a case with a specific disruption duration ranging from 1 to 24 h.

The *WNE* when all nodes are disrupted in a certain time slot firstly decreases and then increases with the disruption start time when the duration time is fixed at a value smaller than 7 h; it firstly decreases, then increases, and lastly fluctuating increase when the duration time is fixed at a value greater than 7 h (see Fig. 5). For example, when the disruption duration is set as 2 h, the *WNE* when all nodes are disrupted slightly decreases from 0.07938 with the start time of 0:00 to 0.0772 with the start time of 5:00, and then to 0.0614 with the start time of 11:00, and then increases to 0.0789 with the start time of 23:00. When the disruption duration is set as 12 h, the *WNE* when all nodes are disrupted decreases from 0.0572 with the start time of 0:00 to 0.0047 with the start time of 8:00, and then increases to 0.0683 with the start time of 20:00, and lastly decreases to 0.050 with the start time of 23:00. The most influential start time is 12:00 when the disruption duration is 1 or 4 h; 11:00 when the disruption duration is 2, or 5 h; 10:00 when the disruption duration is 3, 6, 7 or 8 h; 9:00 when the disruption duration is 9 or 10 h; 8:00 when the disruption duration is 11 or 12 h; 7:00 when the disruption duration is 13, 14, or 15 h, 6:00 when the disruption duration is 16 h; 5:00 when the disruption duration is 17,18 or 19 h; 4:00 when the disruption duration is larger than 19 h. Overall, the start time with the lowest value of *WNE* keeps advancing with the increase of disruption duration, and the disruptions affecting the period 12:00–13:00 has a relatively higher influence on network performance than the others with the same disruption duration.

The shorter the disruption duration is, the more robust the HSR network is. This means the *WNE* in scenarios with shorter disruption duration is greater than that with longer durations (see Fig. 5). Specifically, the *WNE* in the scenarios with 1-hour disruption duration is all greater than those with longer durations.

4.2. *Effect of disruption duration*

Fig. 6 shows the relationship between *WNE* and disruption duration. Each curve represents a specific disruption start time. The

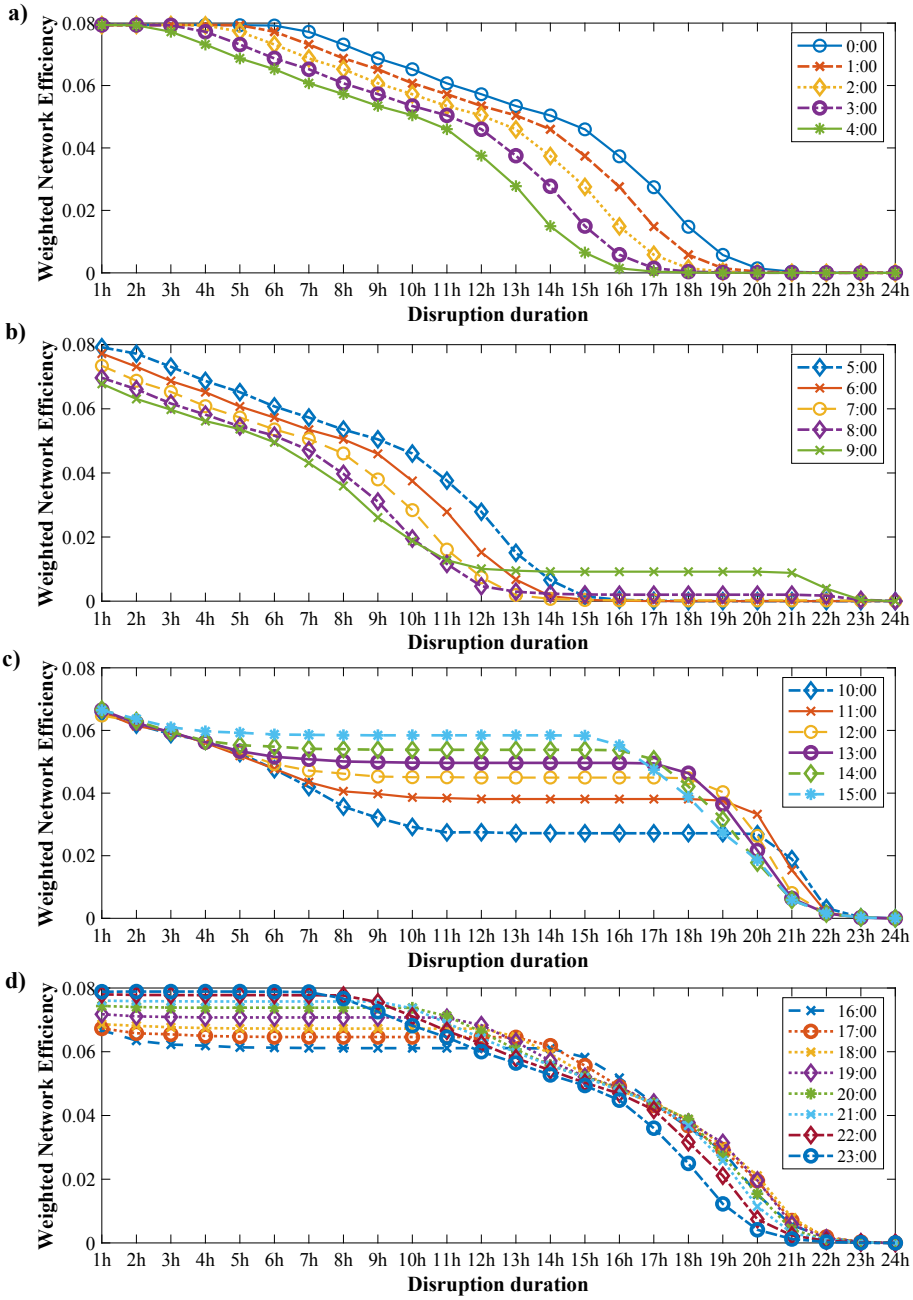

Fig. 6. The weighted network efficiency (*WNE*) with different disruption durations.

subfigures Fig. 6 (a), (b), (c), and (d) show the cases with a start time between 0:00–4:00, 5:00–9:00, 10:00–15:00, and 16:00–23:00, respectively.

As shown in Fig. 6, the *WNE* generally exhibits a decreasing trend when the disruption duration increases from 1 h to 24 h, for any given start time. But the decreasing rate varies with different start times. Some similar trends can be observed in each group. Fig. 6(a) shows that when the disruption starts between 0:00 and 4:00, the *WNE* firstly keeps at a steady level, decreases linearly, and then decreases slowly to a steady level. For example, when the start time is 1:00, the *WNE* keeps steadily at 0.0793 with the disruption duration between 1 h and 5 h, and then decreases linearly to 0.046 with the disruption duration of 14 h, and then decreases dramatically to 0.0014 with the disruption duration of 20 h, and then slowly decreases to zero with the disruption duration of 24 h.

Fig. 6(b) shows that when the disruption starts between 5:00–9:00, the *WNE* firstly decreases linearly, and then decreases exponentially, and then keeps at a steady level, along with the increase in disruption duration. For example, when the start time is 7:00, the *WNE* firstly decreases linearly from 0.0734 with the disruption duration of 1 h, to 0.0461 with the disruption duration of 8 h, and then

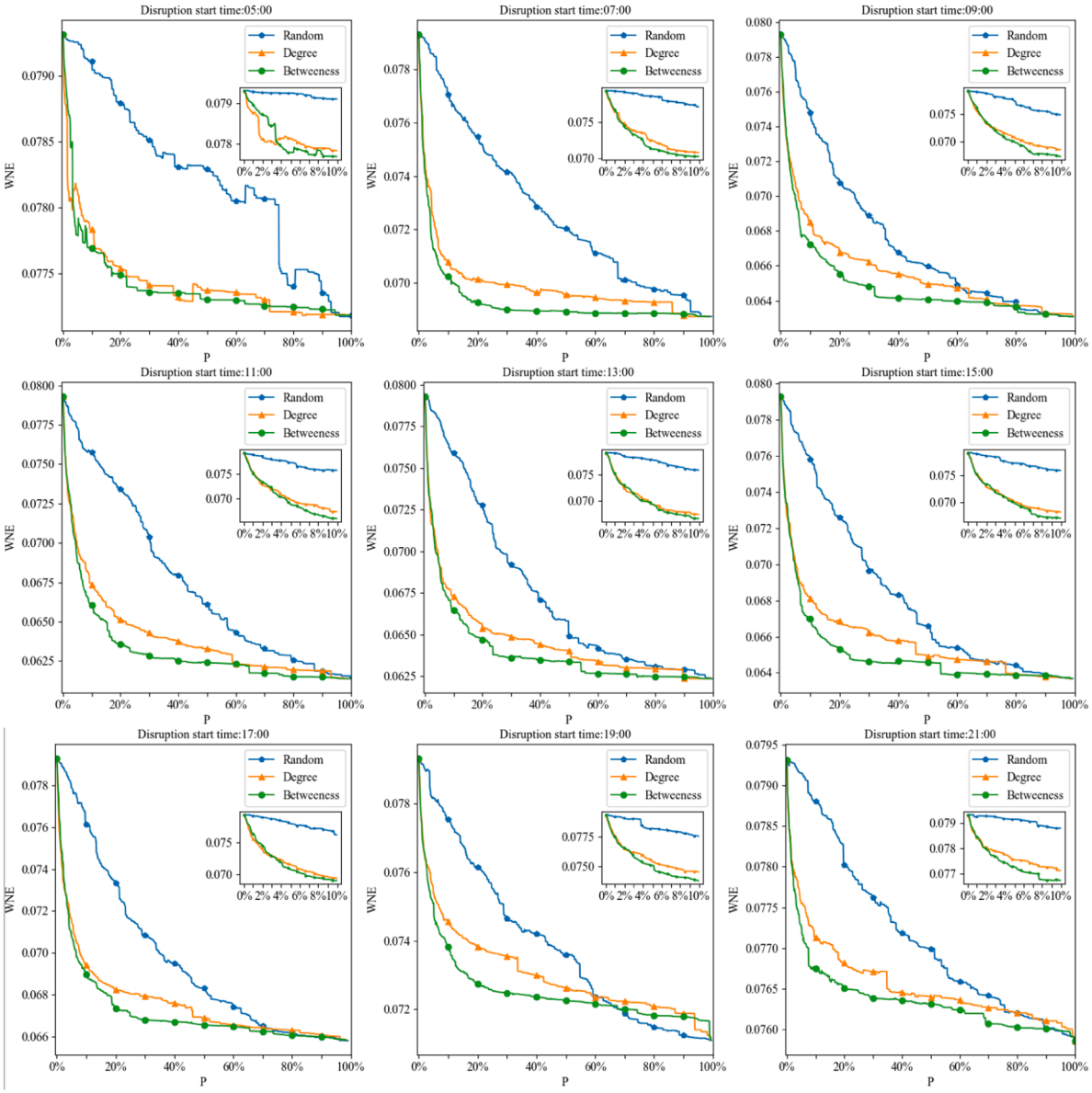

Fig. 7. Robustness of HSR network in different propagation regimes with varying disruption start times (where the disruption duration is fixed as 2 h. *WNE* = weighted network efficiency of HSR network maximal connected subgraph; p = proportion of affected HSR stations in the whole network).

decreases dramatically to 0.0019 with the disruption duration of 13 h, and then slowly decreases to zero with the disruption duration of 24 h.

When the disruption starts between 10:00 and 15:00, as shown in Fig. 6(c), the *WNE* firstly decreases linearly and then decreases slowly to a steady level. For example, when the start time is fixed at 10:00, the *WNE* decreases linearly from 0.0656 (when the disruption duration is 1 h) to 0.0292 (with a disruption duration of 10 h), and then decreases slowly to around 0.0274 (when the disruption duration is between 11 and 14 h), with an overall decrease by 58.6%.

When the disruption starts after 16:00, especially after 20:00, the *WNE* maintains a steady level in the earlier stage, and then gradually decreases and lastly decreases slowly to a steady level, which is similar with that when the disruption starts between 0:00 and 4:00 (see Fig. 6(d)).

Overall, given the same duration of less than 9 h, the disruptions start at 10:00 have the largest influence on network performance. The *WNE* decreases slightly with the increasing disruption duration when the increased disruption duration is within 16:00–4:00, decreases linearly with the increasing disruption duration when the increased disruption duration is within 5:00–9:00, or decreases dramatically when the increased disruption duration is within 10:00–15:00.

5. Effect of disruption propagation regimes

This section examines the impact of failure propagation regimes, including random, malicious and event-led propagation regimes on the network performance. Under the random propagation regime, the sequence HSR stations are disrupted is randomly generated. Under malicious propagation regimes, the sequence is determined by the degree and betweenness centrality of HSR stations in the descending order.[7] The effect of randomly- and maliciously-propagated disruptions are compared under comparable settings. Since the sequence of HSR disruptions under the event-led propagation regime is purely driven by the spread of the particular event and normally cover multiple days, it makes more sense to investigate the effect of this regime under a specific real case, rather than directly comparing with other simulated regimes within a single day. The impact of lockdowns during the COVID-19 outbreak in early 2020 is examined.

5.1. Comparison between random disruption and malicious attack

Regarding the centrality metrics used in the malicious regime, the degree centrality is referred to as the 'strength' of a node in the weighted network, which measures the sum of weights of its adjacencies in a network and is defined by the total number of HSR services operating on the edges that are connected with the node (Jiao et al., 2017; 2020). The betweenness centrality measures the extent to which a particular node lies between other nodes and is measured by the proportion of shortest paths passing a particular node in all the shortest paths between any two nodes (Freeman, 1979). In the weighted network, the shortest topological paths are commonly weighted by service frequencies. Thus, two nodes are considered closer to each other if there are more frequent HSR services between them (Opsahl et al., 2010; Zhou et al., 2019). The degree centrality and betweenness respectively reflect the importance and transitivity of nodes in the HSR network. Overall, three propagation regimes, namely random, degree-based, and betweenness-based regimes, are examined and compared.

The degree-based propagation regime refers to the scenario where HSR stations are disrupted one-by-one in the sequence of descending degree centrality. The nodes with the largest degree centrality in the initial graph fail firstly, which results in the changes in the edge weight connected it, and then the nodes with the largest degree centrality in the remaining graph are disrupted until all the nodes fail or when the network has isolated nodes only. Similarly, the betweenness-based propagation regime refers to the scenario where HSR stations are disrupted according to the sequence of betweenness centrality in the initial and upgraded graph.

We examine the evolutions of *WNE* when the proportion of disrupted HSR stations in the whole network gradually increases under different propagation regimes. Fig. 7 presents the evolutions of *WNE* with different disruption start times and fixed duration (2 h). Fig. 8 presents those with varying disruption durations and fixed start time (7:00).

Results show that the HSR network is the most resilient to randomly-propagated disruptions than the other two propagation regimes, while the betweenness-based propagation is most effective to reduce the network *WNE* when nodes are disrupted (see Figs. 7 and 8). The same trend is found in most scenarios, except that when starting at 5:00 and less than 3% stations are disrupted, the network is more resilient to betweenness-based than degree-based propagation.

A steep fall in the *WNE* occurs when 10% of HSR stations are affected by the betweenness and degree propagation regimes (see Figs. 7, and 8). Specifically, 10% of HSR stations under random propagation reduces the *WNE* in all the time slots when the disruption duration is set as 2 h by no more than 5%, while that under degree-based and betweenness-based propagation reduce the *WNE* by more than 10% when the start time is during 7:00 and 19:00.

The same trend is observed for the robustness assessment across different time slots with random propagation, where the *WNE* decreases with the number of affected nodes. When 10% of HSR stations stopped working, the *WNE* decreases by 5.69% under random propagation when the time slot is 9:00–11:00, which is smaller than that under degree-based (13.62%) and betweenness-based (15.24%) propagation regimes. After the affected nodes increase to 80% or more, the *WNE* decreases slightly. This implies that the robustness against random propagation strongly depends on 80% of HSR stations, which is different from the degree- and betweenness-based regimes (more likely malicious-designed), which depend on 10% of HSR stations.

The evolutions of *WNE* under degree- and betweenness-based propagation regimes demonstrate strong consistency across scenarios with various disruption durations and start times (see Fig. 8). For example, the maximum percentage changes of *WNE* under betweenness- and degree-based regimes both appear in the scenarios where disruption starts at 10:00. The maximum decrease percentage of *WNE* is 17.42% and 15.02% for betweenness- and degree-based regimes, respectively. This means that when the disruption duration is 2 h, malicious disruptions starting at 10:00 might has the largest influence on network performance. Under the random regime, the maximum drop of *WNE,* 5.69%, appears where the start time is 9:00, and 10% of nodes are disrupted.

5.2. Effect of event-led propagation: A case study of the COVID-19 outbreak (early 2020, China)

This subsection examines the impact of lockdowns during the COVID-19 outbreak in early 2020 as a case study of the event-led propagation regime. The Coronavirus Disease 2019 (COVID-19) refers to the cluster of viral pneumonia cases that occurred since December 2019. It was first diagnosed in Wuhan City, Hubei Province, China. The subsequent outbreak of COVID-19 led to the lockdowns of Wuhan City, other cities in Hubei Province, and then many cities around the country in China.

[7] The degree and betweenness centrality are representative indicators of nodal importance and transitivity in the network, respectively (Chen et al., 2020).

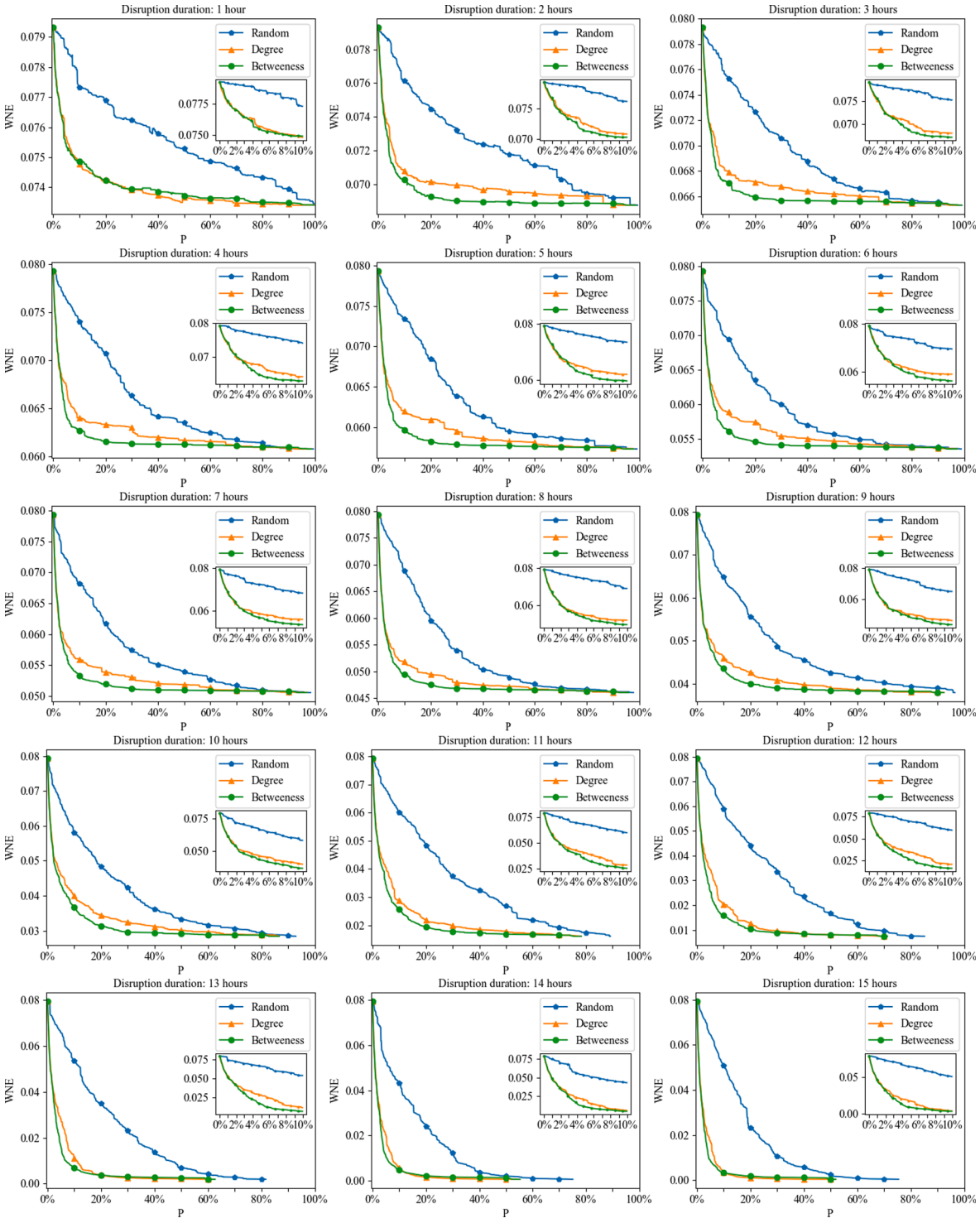

Fig. 8. Robustness of HSR network in different propagation regimes with varying disruption duration (the disruption start time is 7:00; *WNE* = network efficiency of HSR network maximal connected subgraph; P = the proportion of affected HSR stations in the whole network).

One of the lockdown actions is the closure of HSR stations (and all intercity transportation). According to the media news, the HSR stations in Wuhan City were closed from 23 January 2020 to 8 April 2020. Stations in other cities in Hubei Province were mostly closed before 3 February 2020. Some stations in other cities such as Tianjin, Zhejiang, Fujian, Jiangsu, Jiangxi, Heilongjiang, Henan, Shaanxi, Anhui, Liaoning, Sichuan, Guangxi, Jilin, and Hebei provinces were closed from 3 February 2020. After the peak of the COVID-19

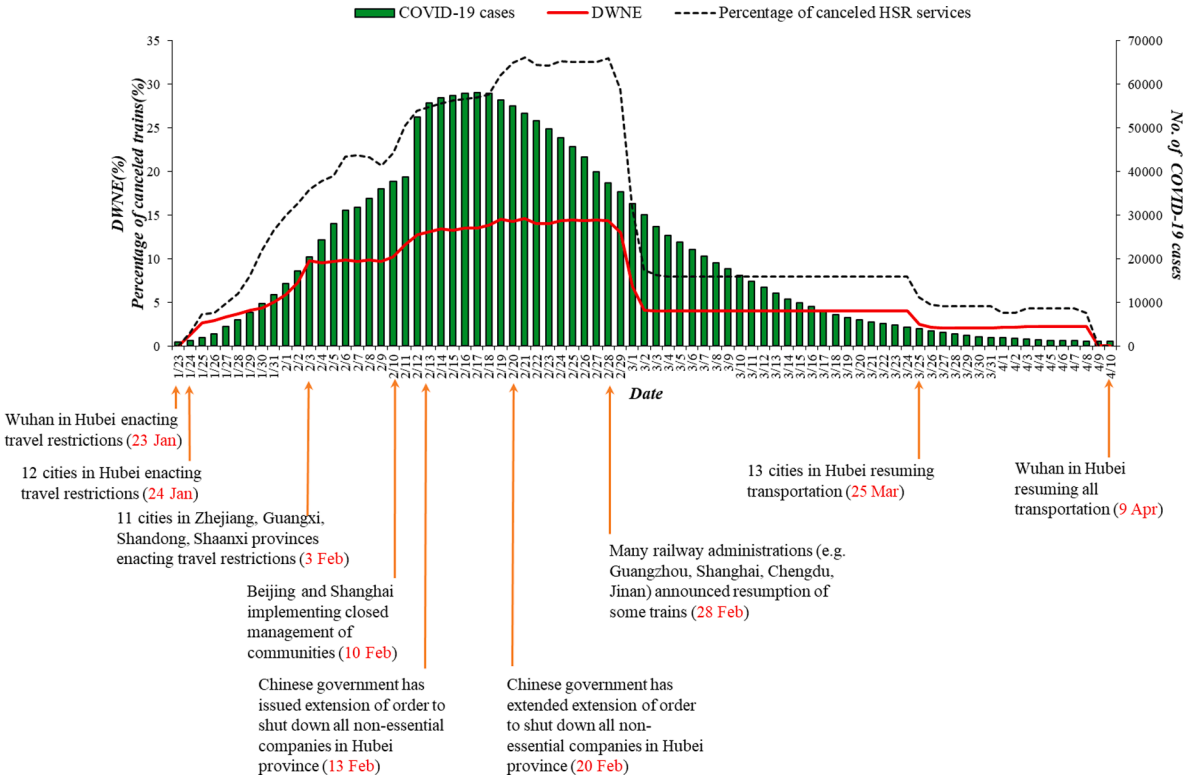

Fig. 9. The percentage changes in WNE (DWNE) caused by COVID-19 from 23 January 2020 to 10 April 2020.

pandemic, transportation, and economic activities gradually resumed. The critical time points are indicated along the time horizon in Fig. 9.

To explore the influence of the COVID-19 outbreak on HSR service, the adjustment information about the HSR service is collected from the China Railway website between December 2019 and April 2020 (https://www.12306.cn/index/, accessed on 28 February and 27 June 2020). The information includes operated HSR service IDs, canceled service IDs, and the corresponding dates. To eliminate the influence of augmented HSR services during the Spring Festival travel rush, the benchmark of *WNE* is calculated based on the regular HSR services before the Spring Festival. Specifically, the HSR services during the lockdown period are compared with those on 31 December 2019. Only those operated on 31 December 2019 but disrupted during the lockdown are taken into the account of reduction of *WNE* (*DWNE*). Compared with the HSR service on 31 December 2019, an accumulation of 2436 services was canceled during the sampling period (23 January-10 April 2020). Most of the service cancelation is observed from the period before 28 February 2020 while only 30 of them occurred thereafter.

Based on the collected HSR service data, we calculate the *WNE* of the HSR network for each day from 23 January-10 April 2020 and the *DWNE* (with reference to 31 December 2019). The evolution of *DWNE* is presented in Fig. 9. To provide more context information, the percentage of canceled HSR services in all services and the total active COVID-19 cases in mainland China on each day is also collected and presented in Fig. 9 for the sampling period. The robustness metric, *DWNE*, is represented by the red solid line, while the other two variables are represented by the dashed line and vertical bars, respectively.

To visualize the spatial distribution of canceled HSR services, we present in Fig. 10 the canceled HSR service network for the three critical periods, 23 January-3 February 2020, 4–10 February 2020, and 11–28 February 2020, respectively. Between each affected O-D pair, the line curvature represents the direction of canceled service, i.e., the clockwise direction along the curvature is canceled during the particular period. The line width represents the number of canceled services on a particular route. To delineate the evolution over time, we only present those newly affected in the specific period in subsequent subfigures. Specifically, Fig. 10(a) contain all the canceled services from 23 January-3 February 2020; those shown in Fig. 10(b) represent the newly canceled services during 4–10 February 2020 (which were not affect earlier); and only those being newly affected during 11–28 February 2020 are presented in Fig. 10(c).

It is shown that there are several stages in the evolution of *DWNE* during the sampling period. In the first stage (23 January-3 February 2020), *DWNE* (solid line in Fig. 9) sharply increased to 9.75% at an increasing rate. During this period, the active COVID-19 cases (green bar in Fig. 9) surged to 20,438; 15 cities in Hubei Province (including Wuhan City) and 12 cities in Zhejiang, Guangxi, Shaanxi, Anhui, and Shandong provinces were locked-down successively; 1104 HSR services were canceled and the canceled HSR services are mostly connecting Wuhan City with the other HSR stations located along the Beijing-Guangzhou and Shanghai-Chongqing corridors (shown in Fig. 10(a)). Since the canceled services are mostly concentrated around a hub node, Wuhan, the

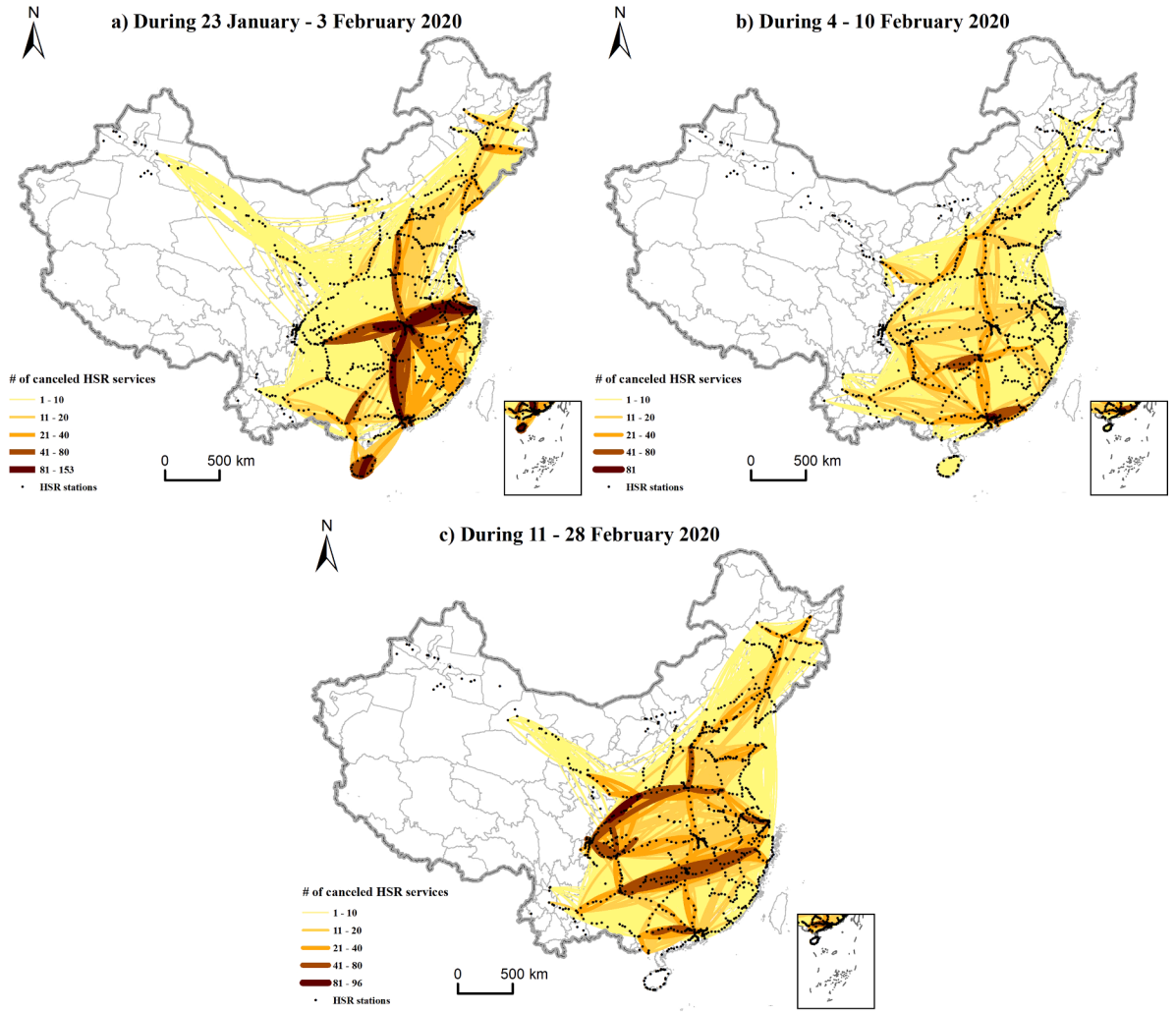

Fig. 10. Spatial distributions of canceled HSR services by COVID-19 from 23 January 2020 to 28 February 2020.

reduction effect on the overall network efficiency is significant.

In the second stage (4–10 February 2020), *DWNE* slightly increased to 10.19%. During this period, the active COVID-19 cases increased to 37,626; and more and more cities and districts were locked-down and most of these cities are located in Zhejiang, Fujian, Jiangsu, Jiangxi, Heilongjiang, Henan, Shaanxi, Anhui, Liaoning, Sichuan, Guangxi, Jilin, and Hebei provinces and Tianjin. Compared with the previous stage, an additional 459 HSR services were canceled during this stage, and most of these HSR services connecting the short travel distance HSR station pairs (i.e. HSR stations in Guangzhou and Shenzhen City as shown in Fig. 10(b)), which has marginal influence on the *WNE*.

In the third stage (10–28 February 2020), *DWNE* firstly increased to 14.57% between 10 and 19 February 2020 and kept steady around 14.33% till 28 February 2020. During this period, the total active COVID-19 in mainland China cases peaked at 58,016 on 17 February 2020 and decreased to 37,414 on 28 February 2020. Although the extended Spring Festival holiday ended on 10 February, more and more cities implemented the closed management of communities (i.e. Beijing and Shanghai) and the Chinese government has issued an extension of order to shut down all non-essential companies in Hubei province on 13 February 2020 and extended it on 20 February 2020, which largely reduced the human mobility and thus affected the service supply. Compared with the previous two stages, another 842 HSR services were canceled in this stage and most of these HSR services were located between HSR stations along the Shanghai-Kunming and Zhengzhou-Chengdu corridors, which are important horizontal transportation corridors. The canceled HSR services along these corridors largely deduced the network performance of the HSR service network.

After 28 February 2020, the HSR service entered the resuming stages. With more and more HSR service resumed operation, the number of canceled HSR services decreased to 1,755 on 29 February 2020, 949 on 1 March 2020, 472 on 7 March 2020, and then kept stable at 472 before 25 March 2020, when 13 cities in Hubei resumed transportation. Thus, the period between 29 February 2020 and 24 March 2020 is defined as the fourth stage, with the *DWNE* decreased from 12.97% to 4.02% and the total active COVID-19 cases decreased from 35,329 to 4,287. The rest of the sampling period is defined as the fifth stage. During the final stage, the *DWNE*

decreased to 2.2% on 8 April 2020 and then to approximately 0, and the total active COVID-19 cases decreasing to 1,089 till 10 April 2020.

Some important implications can be obtained from the observations. Firstly, it is observed from Fig. 9 that prior to the peak of COVID-19 cases, the increasing rate of *DWNE* is larger than that of the active COVID-19 cases. This reflects that the lockdown actions are implemented preceding the increase of active cases. After the peak of COVID-19 cases, the *DWNE* increased slightly and kept stable at a high level and the canceled HSR services did not resume immediately. This reflects the protective strategy the central/local governments adopted in tackling the COVID-19 pandemic.

Secondly, from the spatial distributions of canceled services in Fig. 10, one could infer that the impact of local station closure is marginal compared to large-scale disruption. The closure of HSR stations in Wuhan City is associated (before 26 January 2020) with around 1.3% drop in *WNE* in the national HSR network, even though Wuhan stations are ranked highly according to the simulation scenarios in Section 3 (see Tables 3 and 4). The closure of HSR stations in the other 12 cities of Hubei province is associated with a 1.4% drop in *WNE* in the national HSR network. However, the closure of HSR stations in Tianjin, Zhejiang, Fujian, Jiangsu, Jiangxi, Heilongjiang, Henan, Shaanxi, Anhui, Liaoning, Sichuan, Guangxi, Jilin, and Hebei provinces is associated with about 7% drop in *WNE*.

Thirdly, compared with the scenario considered in Section 3 (Tables 3 and 4) where all services stopping at HSR stations in Wuhan City are suspended, the *DWNE* calculated based on real data is relatively smaller. The difference is caused by the flexibility of service scheduling. Facing station closure, the railway administrations could adjust the service timetable in order to reduce the influence on overall network efficiency. Some services (originally stopping at Wuhan) were modified to passing Wuhan without stopping or to avoid reaching Wuhan. For example, the service G79 from Beijing to Guangzhou was changed to passing Wuhan without stopping; and the service G507 from Beijing West to Hankou was modified to operate from Beijing West to Nanyang East in Henan province (without reaching Wuhan).

More importantly, although exhibiting similar trends, the evolution of *DWNE* does not follow the exactly same pattern as the canceled service percentage. The magnitude of *DWNE* is also different from that of the canceled service percentage. This demonstrates the advantage of the composite metric, *DWNE*. While the number/percentage of canceled services can only reflect the quantity of service suspension, the composite metric reflects not only the quantity but also the impact magnitude on the generalized travel distance in terms of travel time and service frequency. Thus, the proposed metric, *DWNE*, is a plausible tool in comprehensive network robustness analysis to generate more significant managerial insights.

6. Conclusions and policy implications

This study proposes a new framework to assess the robustness of the HSR network influenced by service disruptions occurring in different time and space dimensions. We model the HSR network based on Space-P topological theory where disruptions change weights of edges instead of removing and losing all information related to the affected edges. The weighted efficiency metric is then introduced to evaluate the overall influence of disruptions on the network structure. Two types of disruption propagation regimes, including the random, and malicious propagation regimes, are considered and analyzed. Amongst, for the malicious propagation regime, the status of nodes in the network is evaluated using strength and weighted betweenness centrality, indicating the importance and transitivity of nodes in the weighted network for the degree-based and betweenness-based regimes, respectively. Taking China's HSR network as a case study, we examine the robustness of the HSR network with disruptions that occur at various times of day and geographical locations.

The main findings of this study include:

1) HSR service disruptions happen in East China, in the Yangtze River Delta, or along the Harbin-Hong Kong corridor have the most significant influence on the network performance. HSR stations in Wuhan City play important role in the national HSR network; although the number of stations only accounts for 1.6% of the national total, disruptions of these stations may lead to a 14.33% decrease in the overall *WNE* of China's HSR network, which is greater than many other transportation hub cities (e.g., Beijing, Guangzhou, Nanjing, and Shenyang).
2) The HSR stations with the top 10 decrease in *WNE* vary across different time slots. The critical stations, i.e. Guangzhou South, Nanjing South, Chengdu East, Hankou (a station in Wuhan City), Shijiazhuang, Xi'an North, Wuhan, and Zhengzhou East stations, play important roles in the network performance of the HSR network and are mostly located at the intersections of multiple HSR lines.
3) The robustness of the HSR network is sensitive to the disruption duration and start time. The HSR network in China is less robust with disruptions starting at 10:00 (among those ends within 9 h), or those with longer duration, especially those during 10:00–15:00. The critical time slots show large similarity with the daily frequency of operating HSR services over time, indicating that modifications of service timetable can be potentially effective in enhancing the robustness of the HSR network over time.
4) In terms of how the disruption propagates, the HSR network is the most resilient under random propagation regime, and less robust under the betweenness-based propagation regime in all time slots. It indicates that there may be a consistent pattern of robustness in the HSR network across different time slots. The robustness under random propagation depends on 80% of HSR stations, but that under degree-based and betweenness-based regimes depend substantially on 10% of HSR stations, which is different from the air transport network in China where the network will collapse when 20% of nodes are disrupted under the betweenness-based regime (Chen et al., 2020).
5) According to real data, the impact of lockdowns during the COVID-19 outbreak in early 2020 led to approximately 14.5% reduction of the overall network efficiency at the peak. The evolutions of DWNE and COVID-19 cases indicate that central and local

governments have adopted the aggressive strategy in cooling down transportation and human mobility when facing the increase of COVID-19 cases; after the peak of COVID-19 cases, the protective strategy is adopted to resume HSR services gradually, lagging behind the decline of COVID-19 cases.

This study implies it is necessary to research the robustness of the HSR network with both spatial and temporal variations of disruptions as time-of-day and geographical characteristics have significant influences on the network performance of the overall HSR network. The results demonstrate that the setting of technical standards of HSR infrastructure needs to take into account the variations to enhance the robustness of the overall network. This study provides methodological tools to facilitate decision-makers cognize the robustness of the HSR network with various types of disruptions. It can potentially provide policy supports for new HSR infrastructure planning and the uplift of security protections in critical areas, lines, and stations.

There are some limitations in this work, which present opportunities for future research. First, the proposed framework in this study is built based on several assumptions to simplify the simulation of robustness assessment. The proposed framework is applicable to analyze and evaluate the cascading disruptions of nodes in a particular time slot, instead of multiple intermittent time slots. Hence, it is necessary to extend the framework to analyze service disruptions happening at more than one time slots.

Second, this study focuses on the cascading disruptions of HSR stations, while the analysis of train/HSR line disruptions can also provide important insights into the overall service network robustness. The challenge of involving specific HSR services /lines of China's HSR lies in the difficulty of retrieving the information regarding which HSR service physically uses which track segment. The HSR service between any two stations does not necessarily go along the shortest topological path in the network; services at different time-of-day for the same origin–destination pair may go along different paths. For example, between Nanjing South and Hangzhou East, the service G1509 stops at Shanghai Hongqiao, but service G1667 goes through Huzhou without passing Shanghai Hongqiao. Moreover, some services may physically pass through a station without stopping. For example, the service G31 from Beijing South to Hangzhou East that may not stop at any intermediate station. This leads to high complexity for data collection and network efficiency analysis in the context of train/line disruptions and deserves a profound study in the future.

Third, while this study focuses on the HSR network, the interactions with air transport, intercity bus, and other transport systems can be explored in a future study. Traditionally, HSR is used as a relieving method for grounded air passengers. For example, Air Canada and VIA Rail have an airline-rail re-protection agreement, which is an emergency backup service for airline cancelations, providing train tickets in lieu of flights to get passengers to their destination (Jiang et al., 2017; Li et al., 2018). Some studies have compared and evaluated the vulnerability of HSR and air transport (Li et al., 2019; Chen and Wang, 2019) and the influence of HSR lines on the demand, price, and supply of air transport (Fu et al., 2012; Jiang and Zhang, 2014; Wan et al., 2016; Zhang et al., 2018, 2019; Wang et al., 2020). However, little attention has been paid to the vulnerability of HSR and air transport from both spatially- and temporally-variant perspectives and the impacts of HSR on the vulnerability of the aviation service network. Future studies can extend the current framework to incorporate multi-modal systems.

Lastly, the methodology for network performance assessment incorporating the other factors including the traveler behaviors, i.e. the ticket price, safety, comfort and the environment benefits from the perspective of energy consumption, CO_2 emission, and economic impacts (Robertson, 2016; Gu et al., 2019; Yang et al., 2020; Zhang et al., 2020) should be considered in the future study.

CRediT authorship contribution statement

Jingjuan Jiao: Conceptualization, Methodology, Data curation, Formal analysis, Funding acquisition, Writing - original draft, Writing - review & editing. **Fangni Zhang:** Conceptualization, Investigation, Methodology, Writing - original draft, Writing - review & editing, Funding acquisition. **Jian Liu:** Conceptualization, Methodology, Data curation, Formal analysis, Writing - review & editing, Project administration.

Declaration of Competing Interest

The authors declare that they have no known competing financial interests or personal relationships that could have appeared to influence the work reported in this paper.

Acknowledgements

The authors would like to thank the anonymous reviewers for their helpful comments, which helped improve both the technical quality and exposition of this paper substantially. We also thank for professor Jiaoe Wang from Institute of Geographic Sciences and Nature Resources Research, Chinese academy of Sciences (Beijing China) for her helpful comments, and Yanan Li and Wangyuqing Ma from Beijing Jiaotong University (Beijing China) for data collection. The study was financially supported by the National Natural Science Foundation of China (Grant No. 41701126), the Ministry of Education of the People's Republic China (Grant No. 17YJC790064), and The University of Hong Kong (Grant No. 202009185002).

Appendix A. Comparison of the results by our method and alternative robustness metrics

To examine the effectiveness and robustness of our method, we compared the results measured by our method and several alternative metrics adopted by previous studies. Alternative metrics include the weighted network efficiency (based on Zhou et al.,

2019′s definition) and four more straightforward network efficiency metrics, i.e., including the average shortest travel time with least transfers (Hong et al., 2019), the network efficiency (adopted by Zhang et al., 2016; Chen et al., 2020), the number of affected trains, and the influenced passengers based on expected demand. The definitions of the alternative metrics are given as follows:

1) Shortest travel time (adopted by Hong et al., 2019), of which the travel distance is set as the travel time between node pairs, is set as the difference of the arrival time at the destination station and the departure time at origin station.

2) Network efficiency (adopted by Zhang et al., 2016; Chen et al., 2020), which is calculated using the average value of the reciprocal of the shortest topological paths between node pairs. In the unweighted network, the network efficiency measures the shortest topological paths between node pairs, which is calculated using the average value of the reciprocal of the shortest topological path length between node pairs (Zhang et al., 2016), written as:

$$E = \frac{2}{n(n-1)} \sum_{i,j=1(i\neq j)}^{n} e_{ij}, e_{ij} = 1/d_{ij} \tag{A.1}$$

where E is the network efficiency metric in the unweighted network; n is the total number of nodes in the network at the initial state; e_{ij} is the path efficiency from origin node i to destination node $j$in the unweighted network; d_{ij} is the travel distance from origin node i to destination node j, which is set as the average value of reciprocal of the shortest topological path length between node pairs in the unweighted network and represented by the number of transfers. It is defined as:

$$d_{ij} = \min_{p\in P_{ij}} \sum_{k\in p} e_k \tag{A.2}$$

where $d_{ij}$is the shortest topological path length and the number of transfers equals $(d_{ij} - 1)$; P_{ij} is a set of paths with the shortest topological path length (or the least number of transfers) linking the origin node i and destination node j; a particular path p consists a series of directed edges from the shortest topological path; each directed edge k along path p is considered as an element of path p (Liu et al., 2020); e_k is set as 1, indicating the presence of directed edge k, when there is an HSR service operating on the directed edge k.

3) Weighted network efficiency (based on Zhou et al., 2019′s definition), of which the travel distance is set as the shortest paths between node pairs is calculated by setting the distance between two adjacent nodes as the reciprocal of train frequency instead of one. Based on this definition, the formula of weighted network efficiency is given by $NE = \frac{2}{n(n-1)} \sum_{i,j=1(i\neq j)}^{n} 1/W_{ij}$, where W_{ij} is the weighted shortest topological path, measuring the travel distances weighted by inverse service frequency from origin node i to destination node j along the shortest path, as defined by Eq. (2).

4) The number of affected HSR services, one of the indicators reflecting the HSR service supply. Note that a more intuitive indicator of HSR service supply is the service capacity measured by the number of seats. However, the data regarding the number of seats per train of China's HSR is inaccessible. Although some scholars (i.e. Wei et al., 2020) try to crawler the remaining ticket data from the open-source website (i.e. https://www.ctrip.com/), the data is of low quality. Thus, in this study, we use the number of affected HSR services to evaluate the influence of disruptions on the supply of HSR services.

5) Affected potential demand. As the capacity and passenger volume data are unavailable for China's HSR, we estimate the influenced potential demand as an approximation of the affected passengers by HSR disruptions. We regard all residents of a city as the potential demand for the HSR service. The disruption of HSR service between a specific O-D pair will potentially influence a proportion of the potential demand, where the proportion is determined by the strength of interactions between the O-D pair. Specifically, the expected potential demand from city a to city b is estimated by:

$$\mathrm{Spatialinteraction}_{ab} = \frac{\mathrm{population}_a * \mathrm{population}_b}{traveldistance_{ab}} \tag{A.3}$$

$$\mathrm{Expectedpotentialdemand}_{ab} = \mathrm{population}_a \times \frac{\mathrm{Spatialinteraction}_{ab}}{\sum_c \mathrm{Spatialinteraction}_{ac}}, \mathrm{b, c} \in \mathrm{S}$$

Eq. (A.3) estimates the spatial interaction between city a and city b based on the Gravity model (Carrothers, 1956; Peters et al., 2014). In Eq. (A.3), $\mathrm{Spatialinteraction}_{ab}$ represents the spatial interaction between city a and city b, $\mathrm{population}_a$and $\mathrm{population}_b$ represent the population size of city a and city b, respectively, and $traveldistance_{ab}$ represents the travel distance between city a and city b. Eq. (A.4) estimates the expected potential demand from city a to city b, which is approximated by the population of city a multiplied by the proportion of $\mathrm{Spatialinteraction}_{ab}$ in the summation of the spatial interactions between city a and all possible destinations of city a, where S represents the destination set of city a by HSR.

The robustness metric, affected potential demand, is defined by the total number of the expected demand of HSR service between the disrupted HSR stations, given by

$$\mathrm{Affectedpotentialdemand} = \sum_a \sum_b \mathrm{Expectedpotentialdemand}_{ab}, \mathrm{a, b} \in R \tag{A.5}$$

where R represents the set of HSR stations affected by the disruption.

Given the above definitions, we evaluate and compare the network performance under the proposed method and alternative metrics, respectively, affected by the same disruption. We consider the typical scenario where a particular HSR station is disrupted by an incident for a whole day. We simulate the scenario for all HSR stations in China and obtain the corresponding robustness metrics

Table A1
Top 20 HSR stations ranked by the proposed metric and alternative metrics.

Rank	Our method (*DWNE*)	Increment of shortest travel time (Hong et al., 2019)	Reduction of network efficiency (Zhang et al., 2016; Chen et al., 2020)	Reduction of weighted network efficiency (Zhou et al., 2019)	No. of affected HSR services	Affected potential demand
1	Guangzhou South	Guangzhou South	Xi'an North	Guangzhou South	Guangzhou South	Guangzhou South
2	Nanjing South	Shanghai South	Urumqi	Nanjing South	Nanjing South	Xi'an North
3	Xi'an North	Hankou	Guangzhou South	Chengdu East	Shanghai Hongqiao	Xuzhou East
4	Hankou	Xi'an North	Shanghai South	Xi'an North	Hangzhou East	Shanghai Hongqiao
5	Shanghai South	Nanjing South	Xuzhou East	Zhengzhou East	Shenzhen North	Chengdu East
6	Chengdu East	Xuzhou East	Lanzhou Xi	Hankou	Changsha South	Beijing Xi
7	Wuhan	Wuhan	Chengdu East	Wuhan	Beijing South	Beijing South
8	Zhengzhou East	Zhengzhou East	Hankou	Changsha South	Zhengzhou East	Chongqing West
9	Xuzhou East	Foshan West	Lianyungang	Kunming South	Xi'an North	Nanjing South
10	Shijiazhuang	Shijiazhuang	Shenyang North	Shanghai South	Wuhan	Shijiazhuang
11	Changsha South	Urumqi	Beijing West	Shijiazhuang	Chengdu East	Hangzhou East
12	Kunming South	Shenyang North	Zhengzhou East	Hangzhou East	Jinan West	Huaian East
13	Urumqi	Changsha South	Wuhan	Lanzhou West	Shijiazhuang	Zhengzhou East
14	Hangzhou East	Hefei South	Shenyang North	Xuzhou East	Xuzhou East	Taiyuan South
15	Foshan West	Lianyungang	Kunming South	Urumqi	Hefei South	Fuyang South
16	Lanzhou West	Beijing West	Shijiazhuang	Shanghai Hongqiao	Nanning East	Chaoyang
17	Beijing West	Tangshan	Beijing South	Shenzhen North	Suzhou	Changsha South
18	Shenyang North	Shenyang	Shanghai Hongqiao	Foshan West	Wenzhou South	Maoming
19	Shenyang	Chengdu East	Nanjing South	Beijing West	Hankou	Suqian
20	Hefei South	Hangzhou East	Tangshan	Shenyang	Wuxi	Hufei South

based on different definitions.

Table A.1 shows the top 20 HSR stations ranked by the proposed metric (*DWNE*) and alternative metrics. While a large proportion of the involved HSR stations appear in all rankings, different metrics give different priority sequences. The largest similarity between the proposed metric and alternative metric lies in the rankings by the reduction of weighted network efficiency (Zhou et al., 2019′s definition). However, rankings of Hankou (a station in Wuhan City), Xuzhou East, Urumqi, Foshan West, and Hefei South stations by *DWNE* are higher than those in the ranking of the reduction of weighted network efficiency (Zhou et al., 2019′s definition). This indicates the potential underestimate of the importance of some non-hub HSR stations if the network efficiency metric does not consider the location-based characteristics of HSR stations, which is evaluated by the average travel time to other stations. Similarly, rankings of HSR stations vary across other metrics.

The similarities of rankings of our method and the shortest travel time (Hong et al., 2019′s definition), and that between our method and the weighted network efficiency (Zhou et al., 2019′s definition) are both 90%, but the included stations are different. For example, Kunming South and Lanzhou West respectively are ranked the 9th and 13th in terms of the methods used by Zhou et al. (2019), but their ranks change to 12th and 16th by *DWNE*. The reason might be that Kunming South and Lanzhou West are located in periphery areas. Compared with other methods, only 50% of the HSR stations amongst the top 20 HSR stations by *DWNE* appear on the list by the number of the affected potential demand. The affected population might overestimate the importance of HSR stations by including the whole population as the potential demand (i.e. Beijing South and Beijing West).

To examine the overall similarity between *DWNE* and alternative metrics, we calculate the correlation coefficients between metrics based on the simulation results obtained for all HSR stations. The correlation coefficients are shown in Table A.2. It is found that the proposed metric has substantial correlations with alternative metrics, with correlation coefficients between 0.61 and 0.98. Some correlation coefficients are negative, as they measure the reduction of network efficiency. The correlation between alternative metrics is also high. This implies that various metrics, capturing different aspects of network efficiency, are consistent with one another in general. In particular, the proposed metric, *DWNE*, is a composite metric that can reflect more comprehensive characteristics of HSR stations in the network, including the topological, service-based, and location-based indicators.

To summarize, the proposed metric *DWNE* is effective and robust as the measurements are consistent with existing metrics. However, *DWNE* is more plausible in generating a more comprehensive appraisal of network efficiency being more inclusive and informative.

Table A2
Correlation of the network efficiency measured by our method and alternative metrics.

	Our method (*DWNE*)	Increment of shortest travel time (Hong et al., 2019)	Reduction of network efficiency (Zhang et al., 2016; Chen et al., 2020)	Reduction of weighted network efficiency (Zhou et al., 2019)	No. of affected HSR services	Affected potential demand
Our method (DWNE)	1					
Increment of shortest travel time (Hong et al., 2019)	0.9202	1				
Reduction of network efficiency (Zhang et al., 2016; Chen et al., 2020)	0.8104	0.8344	1			
Reduction of weighted network efficiency (Zhou et al., 2019)	0.979	0.8269	0.726	1		
No. of affected HSR services	−0.7476	−0.6331	−0.5326	−0.7657	1	
Affected potential demand	−0.6122	−0.5161	−0.512	−0.6158	0.646	1

References

Adjetey-Bahun, K., Birregah, B., Châtelet, E., Planchet, J.L., 2016. A model to quantify the resilience of mass railway transportation systems. Reliab. Eng. Syst. Saf. 153, 1–14.

Cao, X., Lee, L.J.S., 2019. A fast reaction-based port vulnerability assessment against catastrophes: case of the Tianjin Port explosion. Transportation Res. Part A: Policy Pract. 128, 11–33.

Cats, O., Koppenol, G.J., Warnier, M., 2017. Robustness assessment of link capacity reduction for complex networks: application for public transport systems. Reliab. Eng. Syst. Saf. 167, 544–553.

Carrothers, G.A.P., 1956. An historical review of the gravity and potential concepts of human interaction. J. Am. Inst. Planners 22 (2), 94–102.

Chen, Y., Wang, J., Jin, F., 2020. Robustness of China's air transport network from 1975 to 2017. Physica A 539, 122876.

Chen, Z., Wang, Y., 2019. Impacts of severe weather events on high-speed rail and aviation delays. Transportation Res. Part D: Transport Environ. 69, 168–183.

De Bona, A.A., Fonseca, K.V.O., Rosa, M.O., Lüders, R., Delgado, M.R.B.S., 2016. Analysis of public bus transportation of a Brazilian City based on the theory of complex networks using the P-Space. Math. Problems Eng. 2016, 1–12.

Erath, A., Löchl, M., Axhausen, K.W., 2009. Graph-theoretical analysis of the Swiss road and railway networks over time. Networks & Spatial Econ. 9 (3), 379–400.

Freeman, L.C., 1978. Centrality in social networks conceptual clarification. Soc. Netw. 1 (3), 215–239.

Freeman, L.C., 1979. Centrality in social networks. Soc. Netw. 1 (3), 215–239.

Fu, X., Zhang, A., Lei, Z., 2012. Will China's airline industry survive the entry of high-speed rail? Res. Transportation Econ. 35 (1), 13–25.

Gu, P., He, D., Chen, Y., Zegras, P.C., Jiang, Y., 2019. Transit-oriented development and air quality in Chinese cities: A city-level examination. Transportation Res. Part D: Transport Environ. 68, 10–25.

Hong, L., Ye, B., Yan, H., Zhang, H., Ouyang, M., He, X.S., 2019. Spatiotemporal vulnerability analysis of railway systems with heterogeneous train flows. Transportation Res. Part A: Policy Pract. 130, 725–744.

Janić, M., 2018. Modelling the resilience of rail passenger transport networks affected by large-scale disruptive events: the case of HSR (high speed rail). Transportation 45 (4), 1101–1137.

Jiang, R., Lu, Q.C., Peng, Z.R., 2018. A station-based rail transit network vulnerability measure considering land use dependency. J. Transp. Geogr. 66, 10–18.

Jiang, C., D'Alfonso, T., Wan, Y., 2017. Air-rail cooperation: Partnership level, market structure and welfare implications. Transportation Res. Part B: Methodol. 104, 461–482.

Jiang, C., Zhang, A., 2014. Effects of high-speed rail and airline cooperation under hub airport capacity constraint. Transportation Res. Part B: Methodol. 60, 33–49.

Jiao, J., Wang, J., Jin, F., 2017. Impacts of high-speed rail lines on the city network in China. J. Transp. Geogr. 60, 257–266.

Jiao, J., Wang, J., Zhang, F., Jin, F., Liu, W., 2020. Roles of accessibility, connectivity and spatial interdependence in realizing the economic impact of high-speed rail: Evidence from China. Transp. Policy 91, 1–15.

Khaled, A.A., Jin, M., Clarke, D.B., Hoque, M.A., 2015. Train design and routing optimization for evaluating criticality of freight rail road infrastructures. Transportation Res. Part B: Methodol. 71, 71–84.

Li, X., Jiang, C., Wang, K., Ma, J., 2018. Determinants of partnership levels in air-rail cooperation. J. Air Transport Manage. 71 (8), 88–96.

Li, T., Rong, L., Yan, K., 2019. Vulnerability analysis and critical area identification of public transport system: a case of high-speed rail and air transport coupling system in China. Transportation Res. Part A: Policy Pract. 127, 55–70.

Li, T., Rong, L., 2020. A comprehensive method for the robustness assessment of high-speed rail network with operation data: A case in China. Transportation Res. Part A: Policy Pract. 132, 666–681.

Liu, S., Wan, Y., Zhang, A., 2020. Does China's high-speed rail development lead to regional disparities? A network perspective. Transportation Res. Part A: Policy Pract. 138, 299–321.

Lordan, O., Albareda-Sambola, M., 2019. Exact calculation of network robustness. Reliab. Eng. Syst. Saf. 183, 276–280.

Meng, F., Fu, G., Farmani, R., Sweetapple, C., Butler, D., 2018. Topological attributes of network resilience: A study in water distribution systems. Water Res. 143, 376–386.

Opsahl, T., Agneessens, F., Skvoretz, J., 2010. Node centrality in weighted networks: generalizing degree and shortest paths. Social Networks 32, 245–251.

Peters, J.C., Han, E., Peeta, S., DeLaurentis, D., 2014. Analyzing the potential for high-speed rail as part of the multimodal transportation system in the United States' midwest corridor. Int. J. Transp. Sci. Technol. 3 (2), 129–148.

Pien, K.C., Han, K., Shang, W., Majumdar, A., Ochieng, W., 2015. Robustness analysis of the European air traffic network. Transportmetrica A: Transport Sci. 11 (9), 772–792.

Rodríguez-Núñez, E., García-Palomares, J.C., 2014. Measuring the vulnerability of public transport networks. J. Transp. Geogr. 35, 50–63.

Robertson, S., 2016. The potential mitigation of CO_2 emissions via modal substitution of high-speed rail for short-haul air travel from a life cycle perspective–An Australian case study. Transportation Res. Part D: Transport Environ. 46, 365–380.

Sienkiewicz, J., Hołyst, J.A., 2005. Statistical analysis of 22 public transport networks in Poland. Phys. Rev. E 72 (4), 046127.

Sullivan, J.L., Novak, D.C., Aultman-Hall, L., Scott, D.M., 2010. Identifying critical road segments and measuring system-wide robustness in transportation networks with isolating links: A link-based capacity-reduction approach. Transportation Res. Part A: Policy Pract. 44 (5), 323–336.

Sun, L., Huang, Y., Chen, Y., Yao, L., 2018. Vulnerability assessment of urban rail transit based on multi-static weighted method in Beijing, China. Transportation Res. Part A: Policy Pract. 108, 12–24.

Tang, Y., Huang, S., 2019. Assessing seismic vulnerability of urban road networks by a Bayesian network approach. Transportation Res. Part D: Transport Environ. 77, 390–402.
Tillema, T., Van Wee, B., Ettema, D., 2010. The influence of (Toll-Related) travel costs in residential location decisions of households: A stated choice approach. Transportation Res. Part A: Policy Pract. 44 (10), 785–796.
Vansteenwegen, P., Dewilde, T., Burggraeve, S., Cattrysse, D., 2016. Aniterative approach for reducing the impact of infrastructure maintenance on the performance of railway systems. Eur. J. Oper. Res. 252 (1), 39–53.
Wan, Y., Ha, H.K., Yoshida, Y., Zhang, A., 2016. Airlines' reaction to high-speed rail entries: Empirical study of the Northeast Asian market. Transportation Res. Part A: Policy Pract. 94, 532–557.
Wang, K., Jiang, C., Ng, A.K., Zhu, Z., 2020. Air and rail connectivity patterns of major city clusters in China. Transportation Res. Part A: Policy Pract. 139, 35–53.
Wang, Z., Chan, A.P., Yuan, J., Xia, B., Skitmore, M., Li, Q., 2015. Recent advances in modeling the vulnerability of transportation networks. J. Infrastruct. Syst. 21 (2), 06014002.
Wei, S., Jiao, J.J., Wang, L., Xu, J.G., 2020. Evolving characteristics of high-speed railway network structure in Yangtze River Delta, China: the perspective of passenger flows. Appl. Spatial Anal. Policy. https://doi.org/10.1007/s12061-020-09334-7.
Yazdani, A., Otoo, R.A., Jeffrey, P., 2011. Resilience enhancing expansion strategies for water distribution systems: A network theory approach. Environ. Modell. Software 26, 1574–1582.
Yang, X., Yin, H., Wu, J., Qu, Y., Gao, Z., Tang, T., 2019. Recognizing the critical stations in urban rail networks: An analysis method based on the smart-card data. IEEE Intell. Transp. Syst. Mag. 11, 29–35.
Yang, Z., Li, C., Jiao, J., Liu, W., Zhang, F., 2020. On the joint impact of high-speed rail and megalopolis policy on regional economic growth in China. Transp. Policy 99, 20–30.
Yap, M.D., Van, O.N., Van, N.R., Van, A.B., 2018. Identification and quantification of link vulnerability in multi-level public transport networks: a passenger perspective. Transportation 45, 1161–1180.
Ye, Q., Kim, H., 2019. Assessing network vulnerability of heavy rail systems with the impact of partial node failures. Transportation 46, 1591–1614.
Yin, J., Tang, T., Yang, L., Gao, Z., Ran, B., 2016. Energy-efficient metro train rescheduling with uncertain time-variant passenger demands: An approximate dynamic programming approach. Transportation Res. Part B: Methodol. 91, 178–210.
Zhang, J., Hu, F., Wang, S., Dai, Y., Wang, Y., 2016. Structural vulnerability and intervention of high speed railway networks. Physica A 462, 743–751.
Zhang, L., Ma, X., Wang, H., Feng, M., Xue, S., 2013. Modelling and optimisation on bus transport system with graph theory and complex network. Int. J. Comput. Appl. Technol. 48 (1), 83–92.
Zhang, A., Wan, Y., Yang, H., 2019. Impacts of high-speed rail on airlines, airports and regional economies: A survey of recent research. Transp. Policy 81, A1–A19.
Zhang, F., Graham, D.J., Wong, M.S.C., 2018. Quantifying the substitutability and complementarity between high-speed rail and air transport. Transportation Res. Part A: Policy Pract. 118, 191–215.
Zhang, F., Yang, Z., Jiao, J., Liu, W., Wu, W., 2020. The effects of high-speed rail development on regional equity in China. Transportation Res. Part A: Policy Pract. 141, 180–202.
Zhang, W., Pei, W., Guo, T., 2014. An efficient method of robustness analysis for power grid under cascading failure. Saf. Sci. 64, 121–126.
Zhou, Y., Wang, J., Huang, G.Q., 2019. Efficiency and robustness of weighted air transport networks. Transportation Res. Part E: Logistics Transportation Rev. 122, 14–26.
Zhu, Z., Zhou, J., Li, P., et al., 2008. An evolutionary model of urban bus transport network based on B-space. Chin. Phys. B 17 (8), 2874–2880.